Bachelor Project

Czech Technical University in Prague

F3

Faculty of Electrical Engineering
Department of Circuit Theory

Sensorless Field Oriented Control of a Brushless DC Motor

Byron Pitsillis Schutte

Supervisor: doc. Ing. Radoslav Bortel, Ph.D.
Field of study: Electrical Engineering and Computer Science
August 2021

BACHELOR'S THESIS ASSIGNMENT

I. Personal and study details

Student's name: **Pitsillis Schutte Byron** Personal ID number: **462178**

Faculty / Institute: **Faculty of Electrical Engineering**

Department / Institute: **Department of Electrical Power Engineering**

Study program: **Electrical Engineering and Computer Science**

II. Bachelor's thesis details

Bachelor's thesis title in English:

Sensorless Field Oriented Control of a Brushless DC Motor

Bachelor's thesis title in Czech:

Bezsenzorové vektorové řízení synchronního bezkomutátorového motoru

Guidelines:

Design and implement a sensorless field oriented control of a brushless DC motor.
- Select a suitable combination of a microcontroller and power electronics.
- Design the controlling electronics and a printed circuit board.
- Design and implement the controlling algorithm for the estimation of the rotor angle and the field oriented control.

Bibliography / sources:

C. Xia.: Permanent Magnet Brushless DC Motor Drivers and Controls. Wiley, 2012.
D.G. Luenberger.: Introduction to Dynamic Systems: Theory, Models, and Applications. John Wiley & Sons, 1979.

Name and workplace of bachelor's thesis supervisor:

doc. Ing. Radoslav Bortel, Ph.D., Department of Circuit Theory, FEE

Name and workplace of second bachelor's thesis supervisor or consultant:

Date of bachelor's thesis assignment: **12.02.2021** Deadline for bachelor thesis submission: **13.08.2021**

Assignment valid until: **30.09.2022**

doc. Ing. Radoslav Bortel, Ph.D. Supervisor's signature	Head of department's signature	prof. Mgr. Petr Páta, Ph.D. Dean's signature

III. Assignment receipt

The student acknowledges that the bachelor's thesis is an individual work. The student must produce his thesis without the assistance of others, with the exception of provided consultations. Within the bachelor's thesis, the author must state the names of consultants and include a list of references.

.	
Date of assignment receipt	Student's signature

Acknowledgements

This Bachelors Thesis was written by Byron P Schutte in the Department of Circuit Theory at the Faculty of Electrical Engineering at the Czech Technical University in Prague.

I would like to thank the following people,

Patrick T Ramos
A good friend and math teacher who supported me throughout my entire degree. I would have not gotten this far without him.

doc. Ing. Radoslav Bortel, Ph.D
My Thesis Supervisor and Signal Theory Professor, it was an absolute pleasure and honor to have worked with him.

doc. Ing. Mattia Butta, Ph. D
My Sensors and Measurement Professor, who took his time to revise my knowledge for the state exam.

And lastly, my parents for their never-ending support.

Declaration

I hereby declare that I have completed this thesis independently and that I have used only the sources (literature and webpages) listed in the enclosed bibliography.

_____

Byron Pitsillis Schutte

[13.08.2021]

Abstract

The aim of this thesis is to design and build an Electric Speed Controller that implements the theory of field orientated control. Using an angular position sensor or current sensing to control a brushless direct current motor with an Angular or Velocity set point.

The work consists of text, figures, and code snippets, describing the theoretical background and implementation of the project. The printed circuit board and schematics were made using Altium designer and the software was written in C using Microchip Studio.

Keywords: Brushless DC Motor, Field Orientated Control, PID, Electric Speed Controller, Feedback Control, Sinusoidal Modulation, Park Transforms, Clarke Transforms, Printed Circuit Board, Low Side Current Sensing, Sensorless Control, Nonlinear Observer

Abstrakt

Cílem této práce je navrhnout a zrealizovat elektronické řízení rychlosti motoru, které využívá teorie vektorového řízení s využitím senzoru úhlu nebo snímání proudů ke kontrole bezkartáčového motoru v režimu řízení úhlu nebo rychlosti.

Práce pozůstává z textu, obrázků a ukázek kódu, které popisují teorií a realizaci projektu. Desky plošných spojů a schema byly vytvořeny pomocí programu Altium Designer a software bol vytvořen v jazyce C v prostředí Microchip Studio.

Klíčová slova: bezkartáčový motor, vektorové řízení, PID, elektronický ovladač rychlosti, zpětnovazební řízení, sinusová modulace, Parkova transformace, Clarkeho transformace, deska plošného spoje, snímání proudu na zemní straně můstku, bezsenzorové řízení, nelineární pozorovatel

Table Contents

List of Tables

List of Figures

List of Acronyms

AC – Alternating Current
ADC – Analog to Digital Converter
BLDC - Brushless Direct Current Motor
BOM – Bill of Materials
CPU – Central Processing Unit
DC -Direct Current
DFLL - Digital Frequency Locked Loop
DTI – Dead Time Insertion
FET - Field Effect Transistor
FOC - Field Orientated Control
FPU – Floating Point Unit
LDO - Low Dropout Linear Fixed Voltage Regulator
LED – Light Emitting Diode
LSB – Least Significant Bit
MOSFET - Metal Oxide Semiconductor Field Effect Transistors
OP Amp -Operation Amplifier
PCB – Printed Circuit Board
PWM -Pulse Width Modulation
SPI - Serial Peripheral Interface

List of Variables

L_s: $Sator\ Inductance\ [H]$

R_s: $Sator\ Resistance\ [\Omega]$

φ_{FL}: $Flux\ Linkage\ [Wb]$

$i_{\alpha/\beta}$: $Alpha\ \&\ Beta\ Currents\ [A]$

$U_{\alpha/\beta}$: $Alpha\ \&\ Beta\ Voltages\ [V]$

ω: $Angular\ Velocity\ [rad/sec]$

θ: $StatorAngle\ [rad]$

$\hat{\theta}$: $Estimated\ Angle\ [rad]$

G: $Observer/OP\ Amp\ Gain\ [-]$

i_A, i_B, i_C: $Measured\ Currents\ [A]$

θ_e: $Electric\ Angle\ [rad]$

θ_m: $Mechanical\ Angle\ [rad]$

N_p: $Number\ of\ Pole\ Pairs$

V_{out}: $Output\ Voltage\ [V]$

Vcc: $Supply\ Voltage\ [V]$

I_{phase}: $Measured\ Current\ in\ a\ Phase\ [A]$

R_f: $Feedback\ Resistor\ [\Omega]$

R_i: $Input\ Resistor\ [\Omega]$

V_{offset}: $Offset\ Voltage\ [V]$

1 Introduction

Due to the decreasing cost of microcontrollers and BLDC (Brushless Direct Current) motors and increased availably many manufactures are now favoring these motors in their products [6]. BLDC motors can operate in a wide range of environments since they are thermally resistant, have no brushes, therefore generate no electrical sparks, require less maintenance than other types of motors, have higher efficacy and have many other favored properties [5].

The global BLDC motor market is expected to grow at a compound annual growth rate of 5.7% from 2021 to 2028, this is driven by the rising trend of Electric Vehicles globally and features such as motorized seats, sunroofs, adjustable mirrors, electric steering and cooling systems.

Global problems such as oil dependency, global warming and environmental pollution are causing governments to implement policies that encourage consumers to buy electric cars which is driving the demand for BLDC motors. These advantages do not just apply to the motor vehicle market, increased demand is also apparent in the Industrial Machinery, Air Conditioning, Aerospace & Transportation Sectors [6].

Due to these facts, it is a good idea for an engineering graduate to be familiar with the basics of BLDC motors, the electrical circuits and algorithms that drive these motors. The aim of this thesis is to design schematics and a printed circuit board (PCD) for an Electric Speed Controller that can implement field orientated control using a sensored and sensor-less configuration with a magnetic angular encoder or current sensing respectively and program the device.

2 Brushless Direct Current Motors

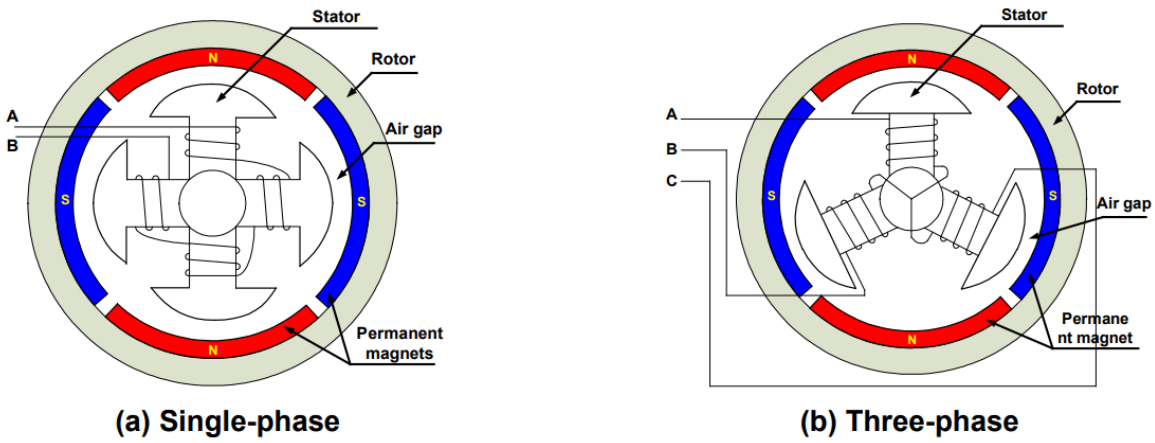

Fig. 1: BLDC Cross Section

BLDC motors are permanent magnet motors, they commonly have three phases with an even number of rotor magnet poles, the number of pole pairs defines the number of electrical revolutions the motor will experience when one mechanical revolution is been applied, knowing the electrical angle of the motor is an important step in calculating the commutation voltages. The more poles a motor will have the greater torque that motor can produce for the same current [9].

To calculate the electric angle of the motor the following equation is used

$$\theta_e = N_p * \theta_m, \qquad (1)$$

where, $\theta_e$is the electric angle, $\theta_m$is the mechanical angle and N_p is the number of pole pairs.

BLDC motors achieves commutation by using position feedback to calculate which switching combination should be engaged. Feedback is usually done with Hall sensors or a rotary encoder but can be estimated by knowing the applied voltages and measuring the currents in the phases.

3 Three Phase Inverter

Three phase inverters consist of 3 pairs of switching elements placed between Vcc and ground, each pair can either connect its respective node to Vcc or ground. These types of inverters can theoretically have 2^6 = 64 different states, some of these sates are not practical. For example such a state where a high and low side switch and closed on the same phase would result in a short circuit and excessive heat would build up in those switching elements. When this inverter is being modulated care must be taken it ensure that switches in the same phase are never closed at the same time, no matter how short the duration is. In this project a three phase inverter was implemented with low side current sensing on each phase, this can be seen in the Fig. 2 [11].

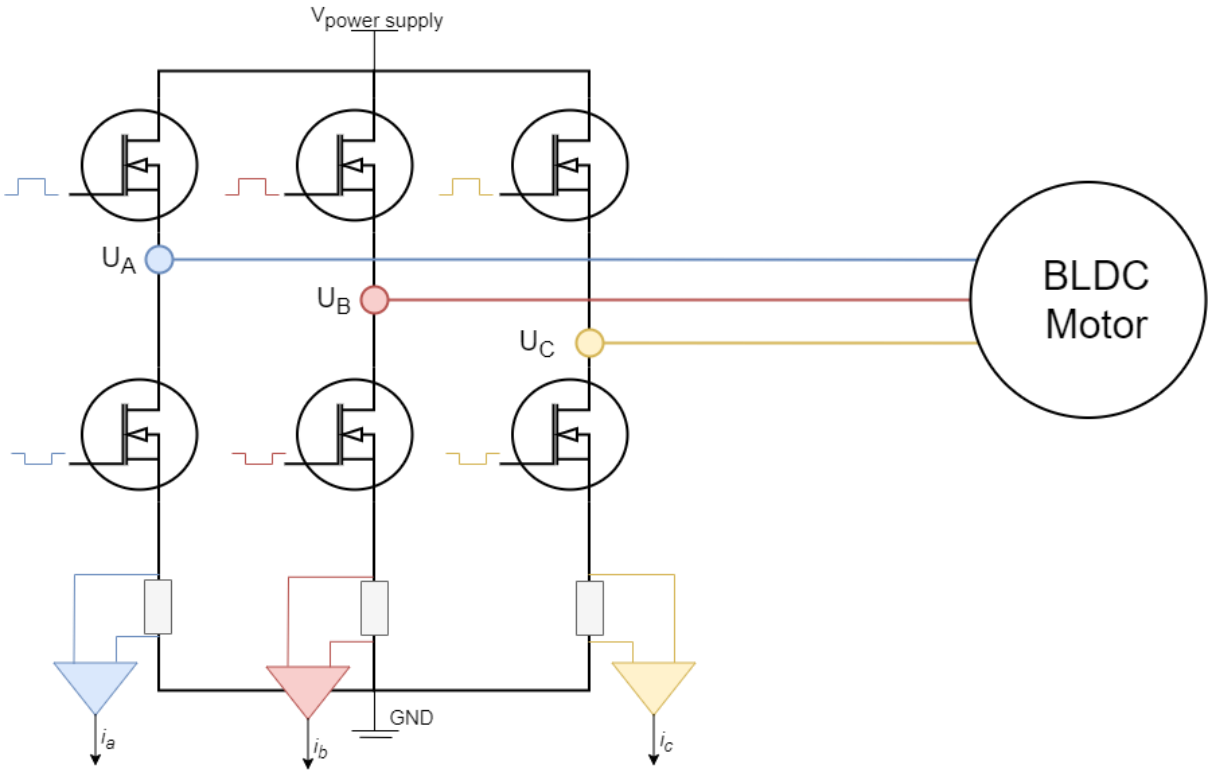

Fig. 2: Three Phase Inverter

3.1 Pulse Width Modulation

Pulse Width Modulation (PWM) is a method to digitally generate an analog signal via the use of high-resolution timers/counters. At any given time, the PWM signal is either high [at the supply voltage] or low [at the ground voltage]. The pulse width also known as the duty cycle. It is directly proportional to the modulated output voltage [8]. If the supply voltage is 12V and the duty cycle is 50% then the average output voltage will be 6V.

The output voltage can be calculated with the following equation

$$V_{out} = Vcc * Duty\ Cycle, \qquad (2)$$

where Vcc is the supply voltage and $Duty\ Cycle$ is a value with range $[0,1]$.

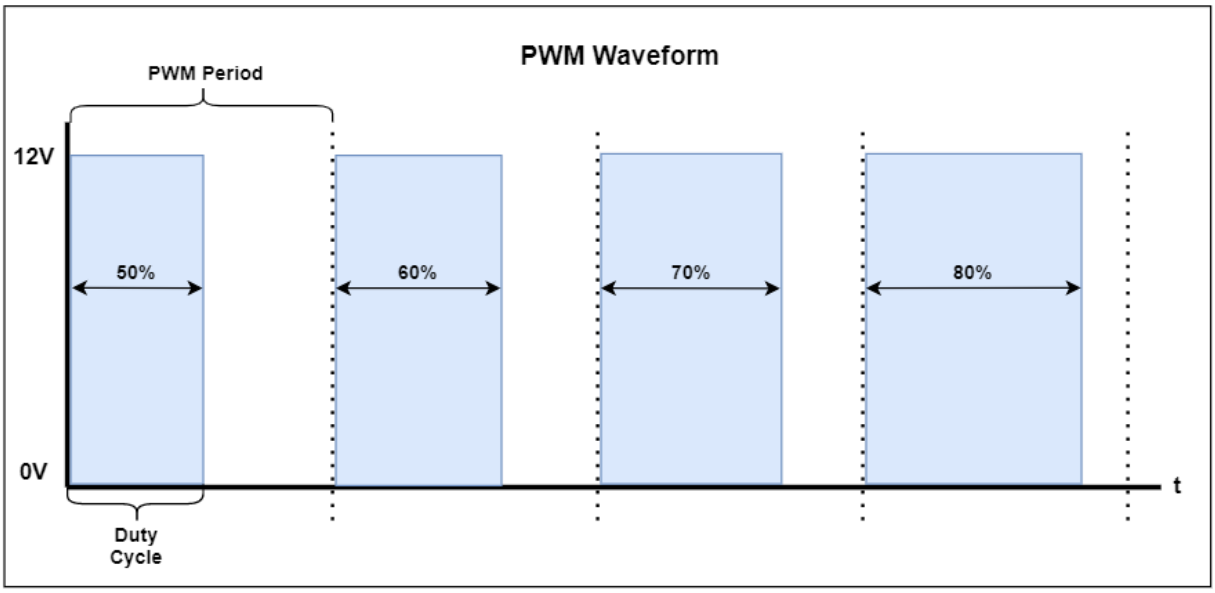

Fig. 3: PWM Waveform

3 separate phase voltages are generated with the timer/counter (TCC0) on the microprocessor. These PWM signals are then modulated on the 3-phase inverter which directly applies the modulated voltage to the motor.

3.2 Dead Time Insertion.

The main objective of Dead Time Insertion (DTI) is to avoid a short circuit between a high side and low side switch that is on the same phase during high frequency switching. This can happen because transistors do not turn on or off instantly. If the switching frequency is fast enough, an overlap may occur where both switches are on at the same time, and excessive heat will occur in the switching components which can lead to permanent damage. The SAMD51 has a built-in dead time insertion block on the PWM generators which was enabled to avoid this problem. [8]

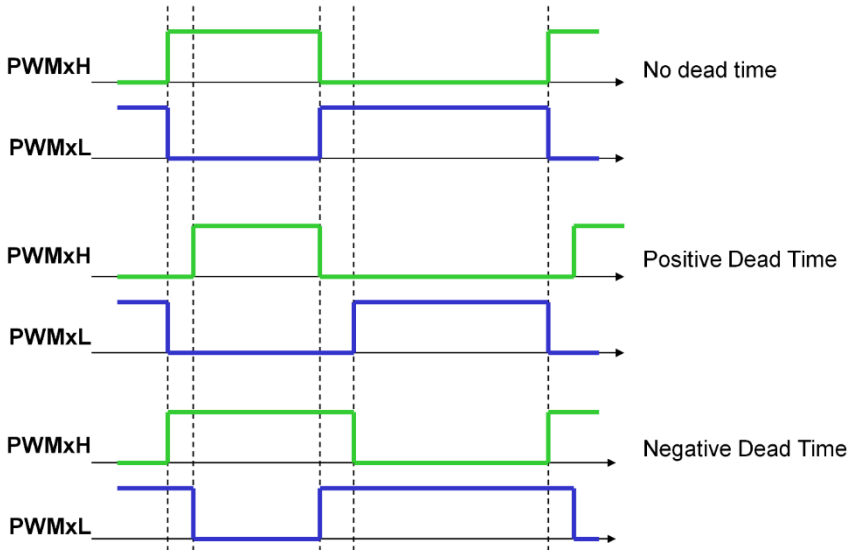

Fig. 4: Dead Time Insertion Wave Forms

4 Field Orientated Control

Field orientated control's goal is to take a defined voltage and a continuously sampled the angle, it then calculates the necessary phase voltages. These phases voltages will generate a magnetic field in the rotor that is rotated by 90 degrees with respect to the permanent magnets on the stator, this creates a torque since the permanent magnets on the stator will be chasing the constantly moving magnetic field.

This can be seeing by observing the equation for magnetic force created by a passing current

$$F = I * B \cdot L \cdot \sin(\varphi), \tag{3}$$

where F $[N]$ is the force experienced, I $[A]$ is the current in the conductor, B $[T]$ is the magnetic field strength, L $[m]$ is the length of the conductor and φ $[rad]$ is the angle between the magnetic field and the current.

The length of the conductor and magnetic field strength of the motor are constant, therefor we are only able to change the angle and current. The angle is constantly read or estimated to achieve

$$\varphi = 90° \; or \; \frac{\pi}{2},$$

since

$$\sin\left(\frac{\pi}{2}\right) = 1.$$

This would result in maximum force and only then the current will affect the force generated by the motor. The current is fed through the motor windings by modulating voltages across the separate phases.

4.1 Sinusoidal PWM

Sinusoidal PWM was implemented in this project. The 3 phase voltages can be calculated using the Inverse Park Transform and Inverse Clarke Transform.

The Inverse Park Transformation is expressed as

$$\begin{aligned} U_{\propto} &= (-1) \cdot U_q \cdot \sin(\theta), \\ U_{\beta} &= U_q \cdot \cos(\theta), \end{aligned} \tag{4}$$

where θ is the electric angle of the motor shaft and U_q is the supply voltage.

The Inverse Clarke Transform is expressed as

$$\begin{aligned} u_a &= U_\propto, \\ u_b &= \frac{(-1)\cdot U_\propto + \sqrt{3}\cdot U_\beta}{2}, \\ u_c &= \frac{(-1)\cdot U_\propto - \sqrt{3}\cdot U_\beta}{2}, \end{aligned} \tag{5}$$

where u_a, u_b and u_c are the phase voltages. These voltages will be pushed into the PWM block.

4.2 Current Sensing

By measuring the currents flowing in each coil, it is possible to determine how much of the current is being put into torque and much is being stored reactively as flux. In order to use the suggested state observer, the currents need to be in the $\alpha\beta$ frame. This is done by using Clarke Transforms [1].

$$\begin{aligned} i_\alpha &= i_A, \\ i_\beta &= \frac{1}{\sqrt{3}}\cdot i_A - \frac{2}{\sqrt{3}}\cdot i_B, \end{aligned} \tag{6}$$

Where i_A, i_B and i_C are the currents from each phase.

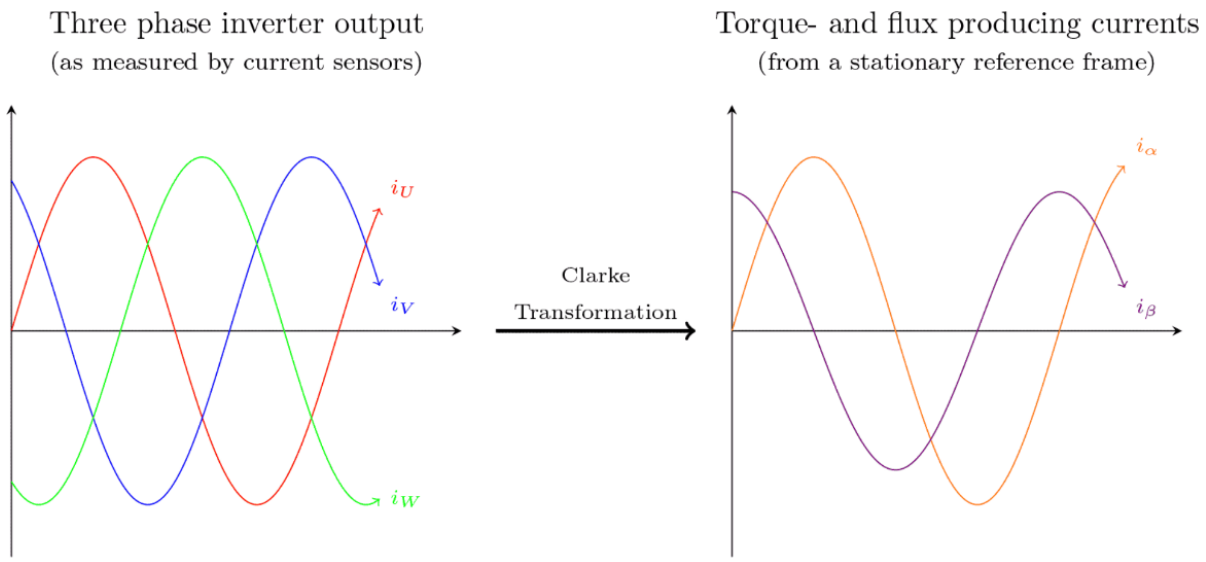

Fig. 5: Clarke Transforms on Currents

5 Types of Rotor Angular Detection

Having a known angle of the stator is essential to solving the FOC equations. The angle can be guessed by using a timestamp to estimate where the rotor will be based off the elapsed time since the last iteration in the control loop. The angle can be measured directly with sensors in or around the motor or, it can be estimated by sensing the currents within the coils and using a state observer function that estimates the angle based off a model of the motor and its operating parameters.

5.1 Time Stamp Estimation

The time stamp method is the simplest method since this does not utilize hardware. The software assumes that the motor is spinning, and based off time stamps between the loop within the program it estimates the angle or velocity of the motor. This method is not accurate and cannot detect if the motor has stalled or if the angle has been changed by an external force. This method has been implemented under "*Velocity/Angle Open Loop*" in the program.

5.2 Angle Sensor

An Angular sensor measures the angle of the shaft. By knowing the angle it is possible to calculate the electric angle and the velocity of the motor. This has been implemented using the AS5048A Magnetic Rotary Encoder and is used when the program is in "*Velocity/Angle Closed Loop*" mode and the *"Sensor Less"* variable is set to false.

5.3 State Observer for Angular Estimation

For some applications, installing position sensors to a motor is troublesome, cost constraints also discourage engineers from using physical sensors, this is where sensor less control is required. This thesis will focus on an observer that uses flux linkage as a state variable, measured voltages and currents in the $\alpha\beta$ frame. Equations and derivations have been sourced from [12].

A BLDC motor with surface mounted rotor magnets can be described in the $\alpha\beta$ frame below.

$$L_s \cdot \begin{bmatrix} \frac{d}{dt} \cdot i_\alpha \\ \frac{d}{dt} \cdot i_\beta \end{bmatrix} = (-1) \cdot R_s \cdot \begin{bmatrix} \mathrm{i}_\alpha \\ \mathrm{i}_\beta \end{bmatrix} + \omega \cdot \varphi_{FL} \cdot \begin{bmatrix} \sin(\theta) \\ (-1) \cdot \cos(\theta) \end{bmatrix} + \begin{bmatrix} U_\alpha \\ U_\beta \end{bmatrix}, \quad (7)$$

where L_s is the stator inductance, R_s is the stator resistance, φ_{FL} is the flux linkage, $\mathrm{i}_{\alpha/\beta}$ are the measured currents in the $\alpha\beta$ frame, $\mathrm{U}_{\alpha/\beta}$ are the applied voltages in the $\mathrm{U}_{\alpha/\beta}$ frame, ω is the angular velocity of the motor which is an unknown and θ is the stator angle which is also unknown.

Observer Construction

$$\hat{x} = \begin{bmatrix} \Phi_{s\alpha} \\ \Phi_{s\beta} \end{bmatrix} = L_s \cdot \begin{bmatrix} \mathrm{i}_\alpha \\ \mathrm{i}_\beta \end{bmatrix} + \varphi_{FL} \cdot \begin{bmatrix} \cos(\theta) \\ \sin(\theta) \end{bmatrix}. \quad (8)$$

Let

$$y \equiv (-1) \cdot R_s \cdot \begin{bmatrix} i_\alpha \\ i_\beta \end{bmatrix} + \begin{bmatrix} u_\alpha \\ u_\beta \end{bmatrix}. \quad (9)$$

The nonlinear part is defined as

$$\eta = \begin{bmatrix} \Phi_{s\alpha} \\ \Phi_{s\beta} \end{bmatrix} - L_s \cdot \begin{bmatrix} \mathrm{i}_\alpha \\ \mathrm{i}_\beta \end{bmatrix} - \varphi_{FL} \cdot \begin{bmatrix} \cos(\theta) \\ \sin(\theta) \end{bmatrix}. \tag{10}$$

The error of the nonlinear component is found by take the norm of η

$$\begin{aligned} \|\eta\|^2 &= {\varphi_{FL}}^2 \\ Error &= {\varphi_{FL}}^2 - \|\eta\|^2. \end{aligned} \tag{11}$$

The observer can then be expressed as

$$\begin{aligned} \dot{x} = \begin{bmatrix} \Phi_{s\alpha} \\ \Phi_{s\beta} \end{bmatrix} &= y + \frac{G}{2} \cdot \eta(\hat{x}) \cdot [{\varphi_{FL}}^2 - \|\eta\|^2], \\ \dot{x} = \begin{bmatrix} \Phi_{s\alpha} \\ \Phi_{s\beta} \end{bmatrix} &= ((-1) \cdot R_s \cdot \begin{bmatrix} i_\alpha \\ i_\beta \end{bmatrix} + \begin{bmatrix} u_\alpha \\ u_\beta \end{bmatrix}) + \frac{G}{2} \cdot \eta(\hat{x}) \cdot [{\varphi_{FL}}^2 - \|\eta\|^2]. \end{aligned} \tag{12}$$

The Stator Angle can be isolated and expressed as

$$\begin{aligned} \frac{1}{\varphi_{FL}} \cdot \left(\hat{x} - L_s \cdot \begin{bmatrix} \mathrm{i}_\alpha \\ \mathrm{i}_\beta \end{bmatrix} \right) &= \begin{bmatrix} \cos(\theta) \\ \sin(\theta) \end{bmatrix} = \tan(\theta), \\ \hat{\theta} &= \tan^{-1}\left(\frac{\Phi_{s\beta} - L_s \cdot i_\beta}{\Phi_{s\alpha} - L_s \cdot i_\alpha}\right), \end{aligned} \tag{13}$$

where $\hat{\theta}$: is the estimate angle and G is the observer gain.

6 Hardware Implementation

6.1 Hardware Block Diagram

Fig. 6 illustrates how the hardware is connected and where hardware signals are fed into software blocks within the Microcontroller.

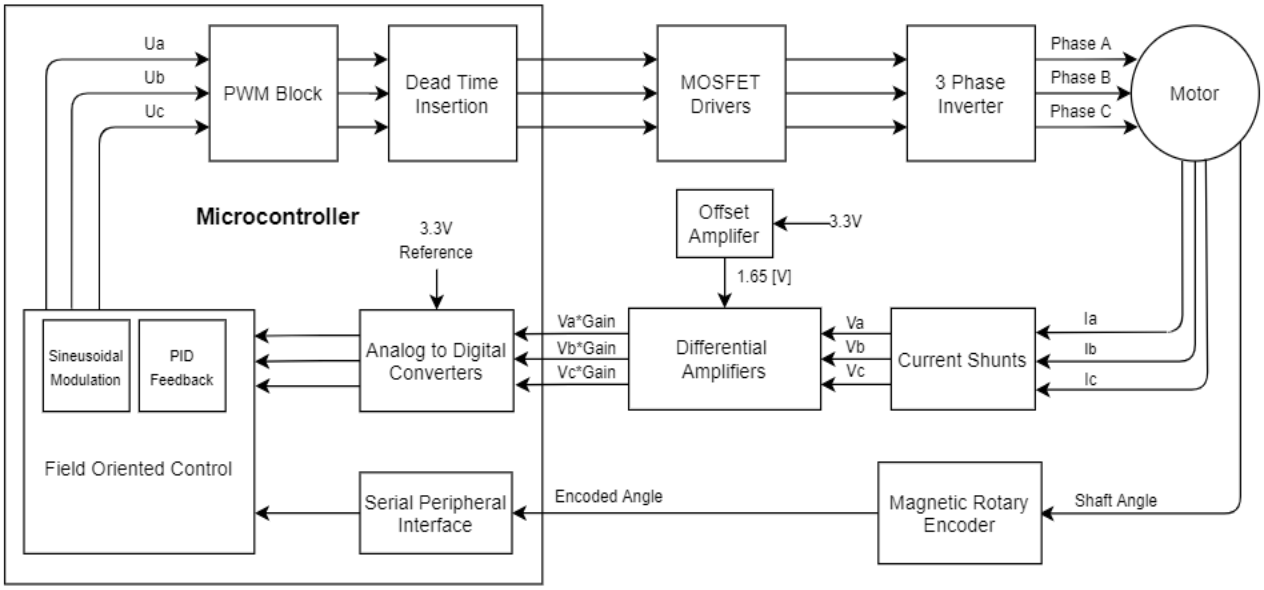

Fig. 6: Hardware Configuration Block Diagram

6.2 Microcontroller

The SAMD51 microcontroller was used, designed by Microchip, it is a 32-bit ARM Cortext M4 based processor with a maximum operating clock frequency of 120MHz. It has a dedicated Floating-Point Unit (FPU) which can be useful for the demanding mathematical operations needed for Field Orientated Control. The chip also has a wide selection of communication interfaces such as SPI and I2C which can be used to interface angle sensors to the device. A full speed USB interface is also available which can be used to monitor and change operating values on the fly via a user interface designed in MATLAB. Out of many timer/counters available on the chip there are two 24 bit timers with 6 compare channels, this allows for great flexibility when generating synchronized pulse width modulation (PWM). These timers also have dead time insertion (DTI) blocks which ensures that the high side and low side switches are never on at the same time. The interrupt flags are also flexible, the user can program when an interrupt is triggered. The chip has one internal 32kHz oscillator, one 48MHz Digital Frequency Locked Loop (DFLL), and two programable Fractional Digital Phase Locked Loop, this gives the programmer huge flexibility with available clock domains within the processor. The MCU has two 12-bit 1 Mega Sample Per Second (MSPS) Analog to Digital Converters (ADCs) with automatic offset and gain error compensation with oversampling support ideal for current sensing.

6.3 Phase Drivers and Transistors

Three Infineon BSC0925ND Metal Oxide Semiconductor Field Effect Transistors (MOSFETs) were implemented in a 3 phase inverter topology. Each of these dual MOSFET packages are driven by an International Rectifier IR2301S high and low side gate driver, implementation can be seen in Fig. 19.

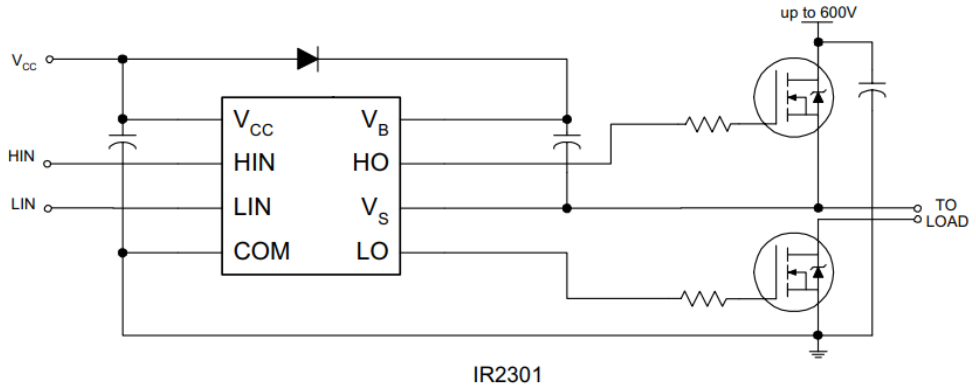

Fig. 7: Phase Driver Schematic

6.4 Power Supply

A P-channel MOSFET has been placed in series with the voltage input connector to provide reverse polarity protection [3]. The ESC board can handle a maximum of 24V on the input terminal, the microprocessor and other components required 3.3V. A Low Dropout Linear Fixed Voltage Regulator (LDO) has been used to generate the 3.3V rail with the necessary decoupling capacitors [4]. A 1000uF capacitor has been placed in parallel between the voltage input and the 3-phase inverter circuit to reduce current ripple from the switching MOSFETs.

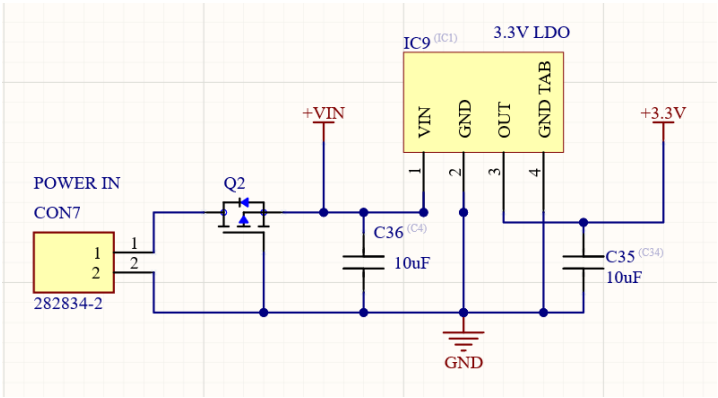

Fig. 8: Power Supply Schematic

6.5 Angular Sensing

The AS5048A Magnetic Rotary Encoder designed by Austria Microsystems was used to measure the mechanical angle of the rotor. It offers 14-bit resolution and is interfaced via SPI communication. The chip contains an array of Hall effect sensors that can detect the change in magnetic field. The zero position can also be programmed, which removes the need to mechanically align the magnet. It is also immune to stray external magnetic fields making it ideal for motor control applications. A small diametrically magnetized magnet is mechanically mounted to the shaft of the motor, the AS5048A is then centered and placed near the magnetic to sense the changes in the magnetic field by the rotating magnet [11].

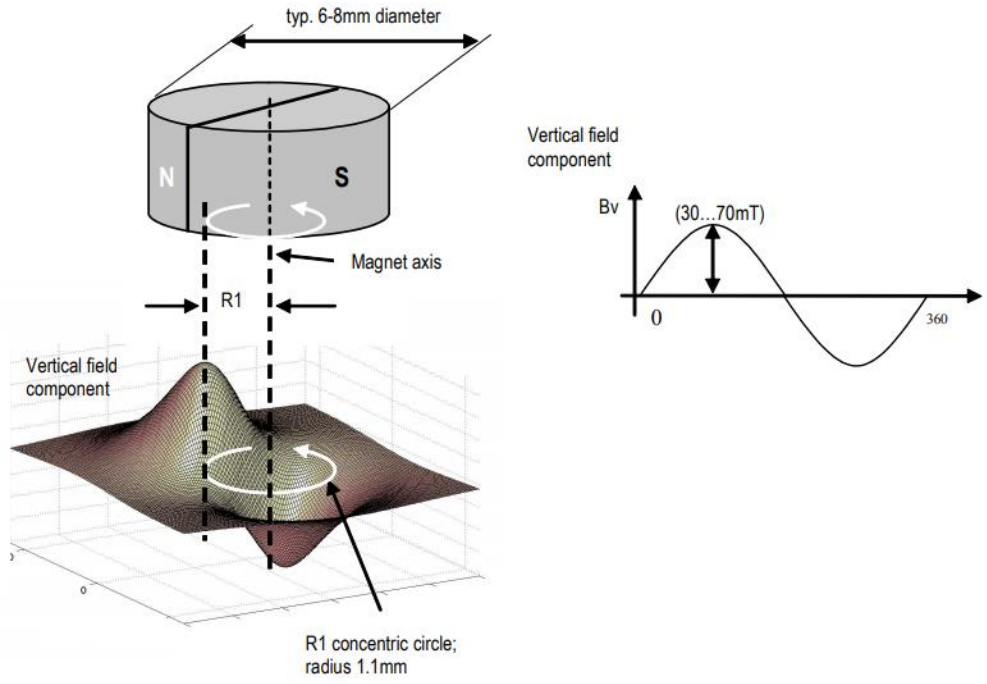

Fig. 9: Magnetic Encoder Theory

6.6 Current Sensing

A Texas Instruments OPA2388 quad operational amplifier (OP Amp) was used for low side current sensing. A shunt resistor has been placed between the low side MOSFETs and ground. Three OP amps were setup in differential mode to measure the voltage drop across $3\ m\Omega$ power sense resistors which can be found on each phase, see Fig. 11. The remaining OP Amp was used to generate a $1.65V$ offset for the current sensing OP Amps, therefor $1.65V \rightarrow 0A$ which can be seen in Fig. 10. The full implementation of these amps can be seen in Fig. 18.

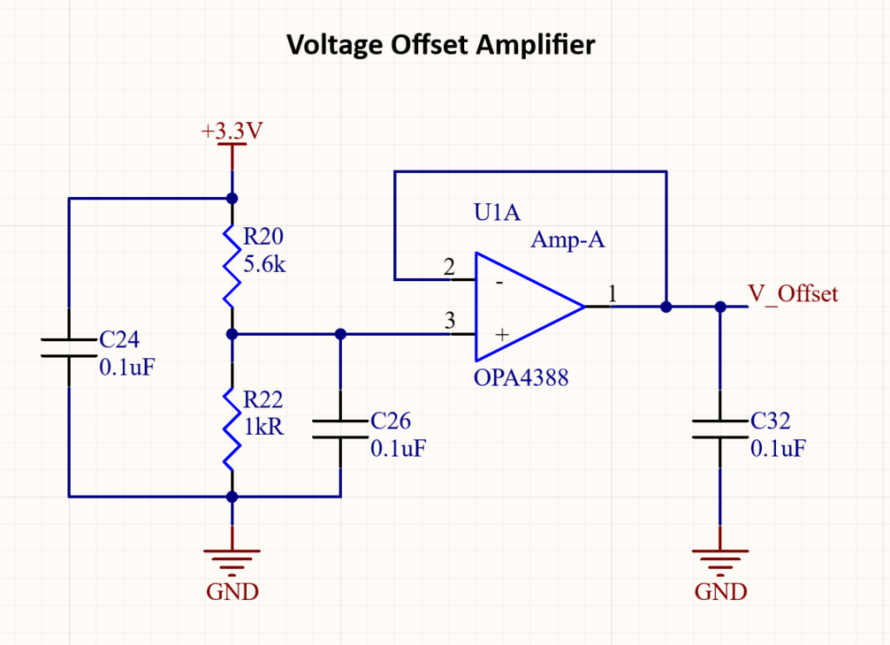

Fig 10: Voltage Offset Amplifier Schematic

The offset can be calculated using the voltage divider equation

$$V_{offset} = V_{cc} \cdot \left(\frac{R_1}{R_1 + R_2}\right)[V]. \tag{14}$$

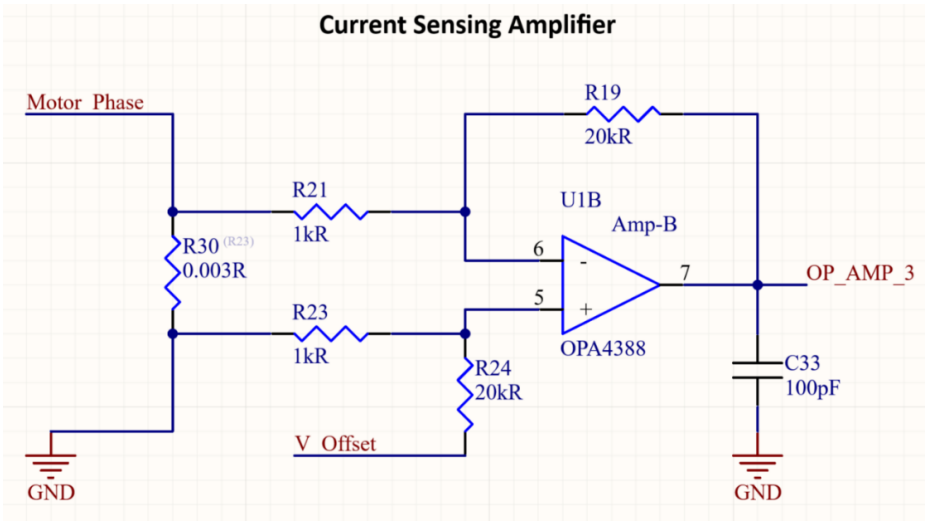

Fig 11: Current Sensing Amplifier Schematic

The output voltage can be expressed as

$$Vout = \frac{R_f}{R_i}\,(V_2 - V_1)\,[V], \tag{15}$$

where the gain is

$$\frac{R_f}{R_i} = \frac{20000}{1000} = 20[-]. \tag{16}$$

The current through the resistor can then be calculated as

$$I_{phase} = \frac{(V_{out} - V_{offset})}{R_{shunt} * Gain}\ [A]. \tag{17}$$

The trick to low side current sensing is that all low side switches must be closed when performing a current measurement. This means that the current sensing function must be synchronized with the PWM generators. This was done by setting the PWM block in *DSBOTTOM* mode, this means that when the counter of the TCC register is zero, an interrupt will be triggered. In other words, this interrupt is serviced when all low side switches are closed, as soon as the interrupt is serviced the program will trigger the ADC to read the voltages from each of the phase [11]. The window when to capture the currents can be seen in Fig. 12.

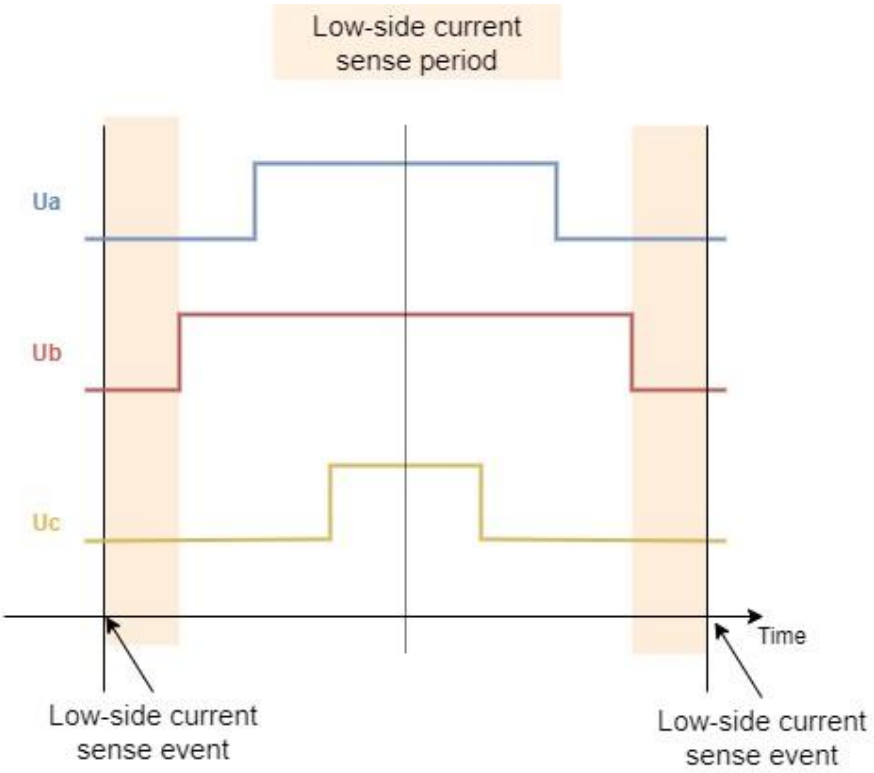

Fig. 12: Low Side Current Capture Waveforms

6.7 Printed Circuit Board

In Fig. 13 is the final Printed Circuit Board (PCB) layout of the ESC. The board measures $82.15mm$ on the X axis and $45.95mm$ on the Y axis

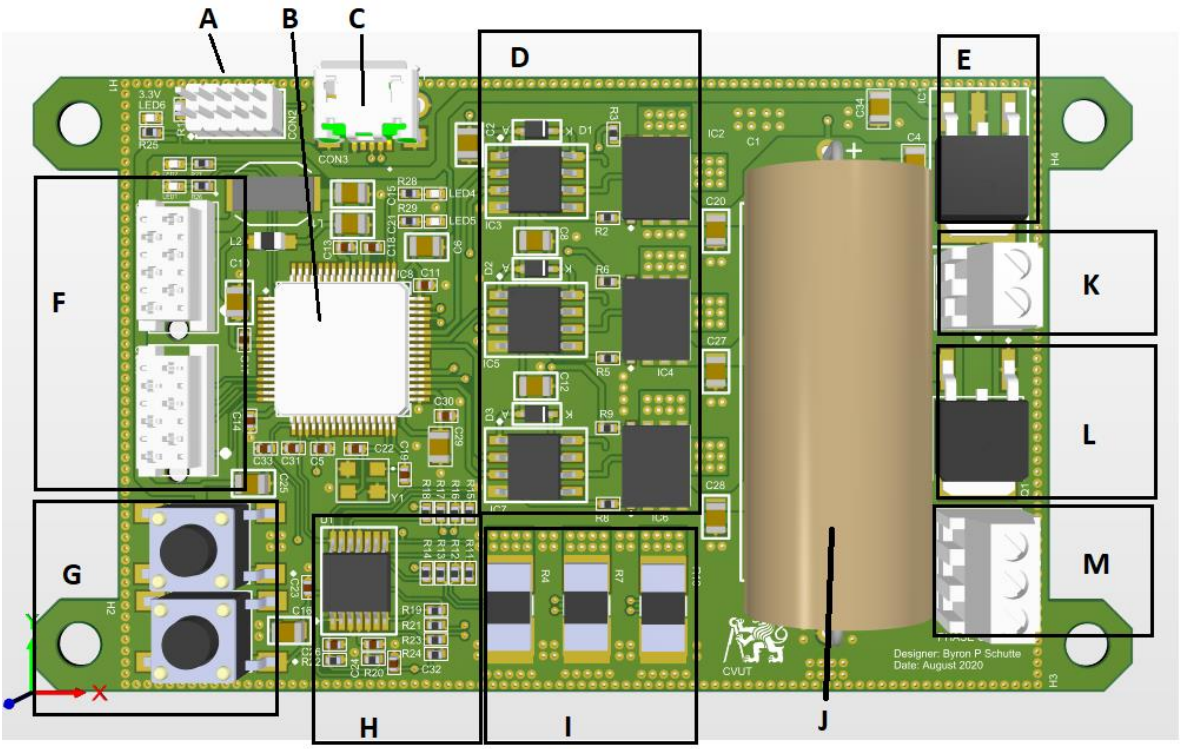

Fig. 13: ESC PCB Board view

A. JTAG Connector for Programming
B. SAMD51 Micro Processor
C. USB Interface
D. MOSFET Drivers and MOSFETs
E. 3.3V Voltage Regulator
F. SERCOM Connectors
G. Push Buttons
H. Quad OP Amp
I. Current Sensing Resistors
J. Smoothing Capacitor
K. Power Connector
L. P Channel MOSFET
M. Motor Connector

6.8 Magnetic Encoder Printed Circuit Board

In Fig. 14 is the final PCB that held the Magnetic Rotary Encoder, this was fitted to a motor mount and would be mounted behind the motor. The board measures $24.02mm$ on the X axis and $11.30mm$ on the Y axis. In Fig. 16 the PCB has been mounted in the motor mount.

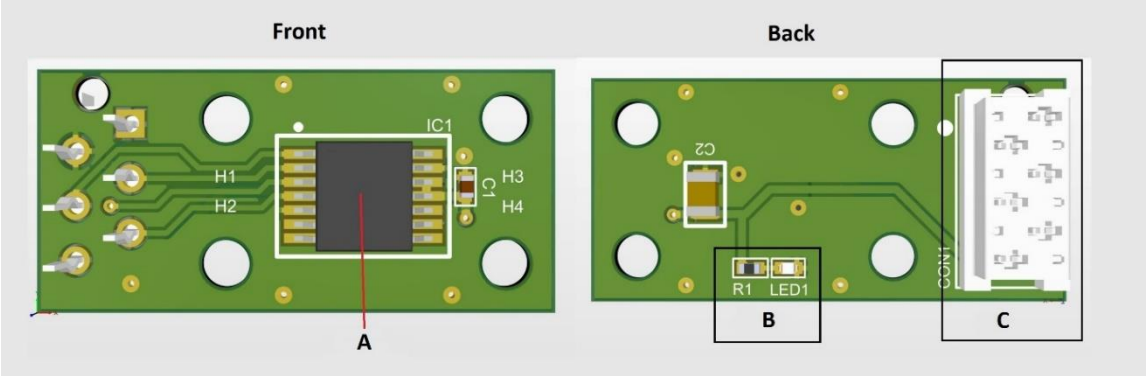

Fig. 14: Magnetic Encoder PCB Board View

A. AS5048A Magnetic Rotary Encoder
B. Power LED
C. Power and Communication Connector

6.9 Motor and Magnet Mount

In Fig. 15 the Motor is shown with the magnet mount and magnet connected to the back of the rotor.

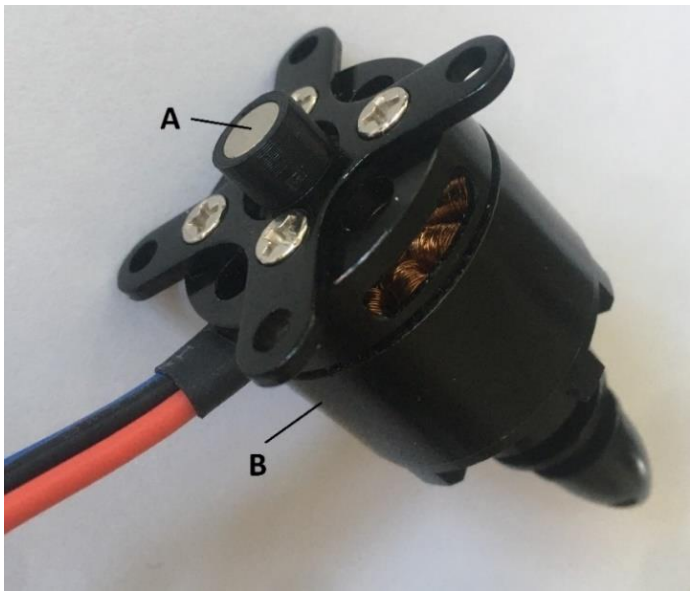

Fig. 15: Motor and Magnet Mount

A. Diametrically Magnetized Magnet
B. BLDC Motor

6.10 Motor Mount and Magnetic Encoder

In Fig. 16 the Magnetic Encoder PCB is seen mounted to the motor mount, when the motor is mounted the magnet will rotate directly above the AS5048A.

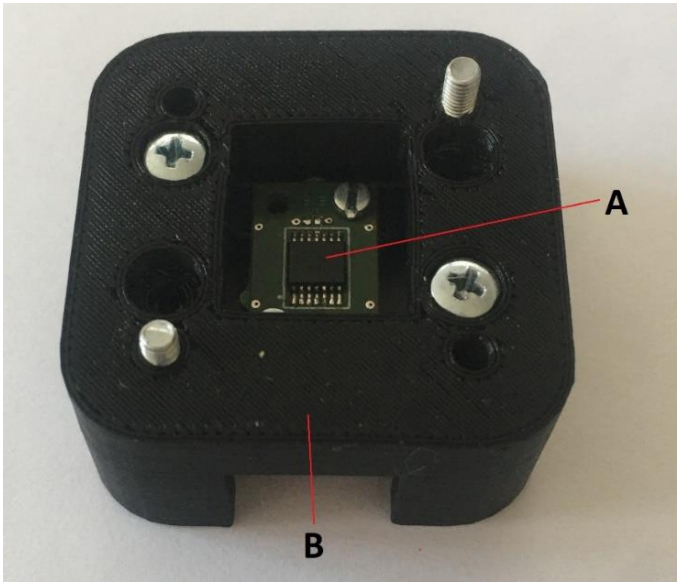

Fig. 16: Motor Mount and Magnetic Encoder PCB

A. AS5048A Magnetic Rotary Encoder
B. Motor Mount

6.11 ESC Schematics

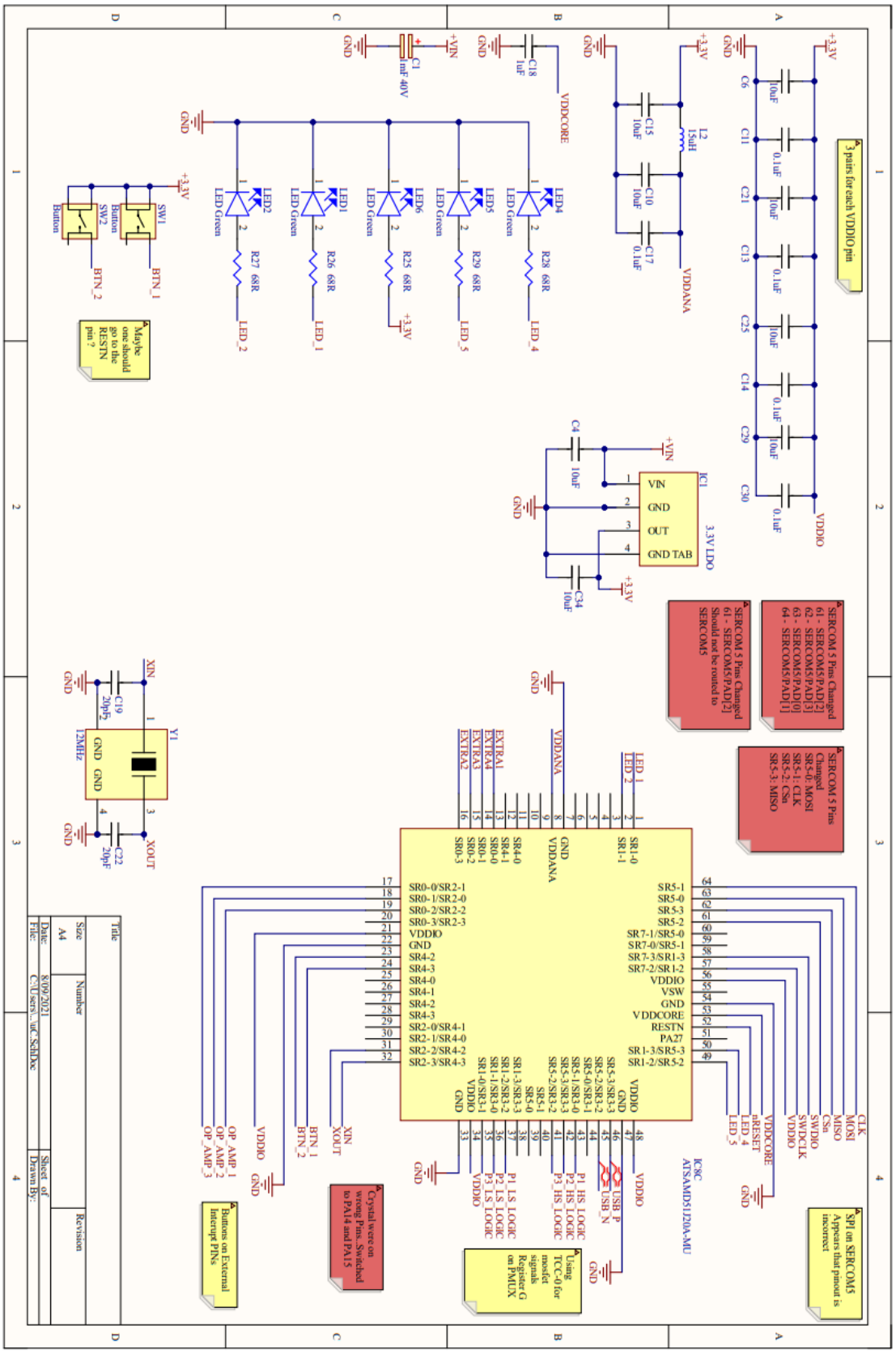

Fig. 17: Microcontroller PCB Schematic

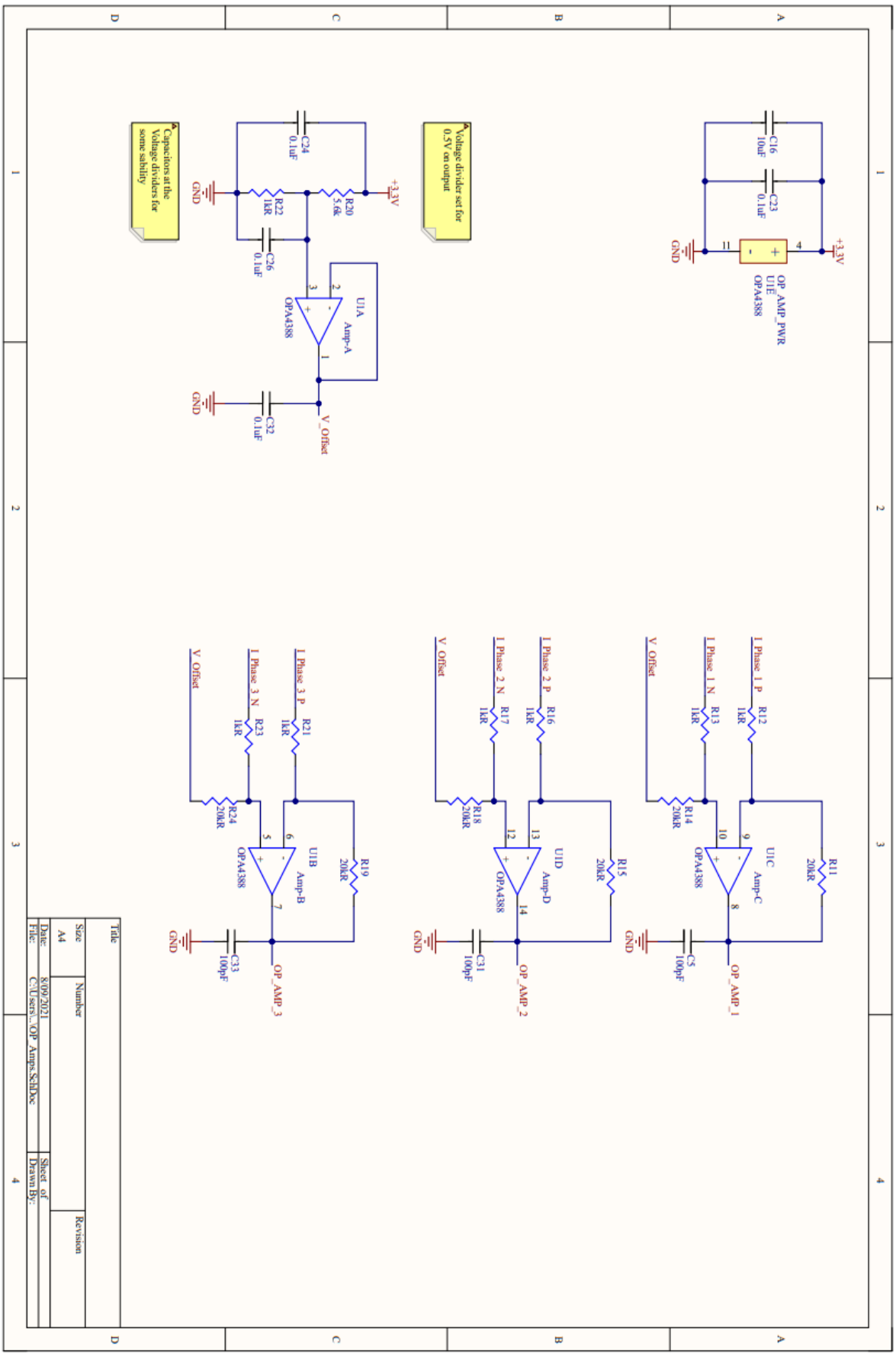

Fig. 18: Operational Amplifiers PCB Schematic

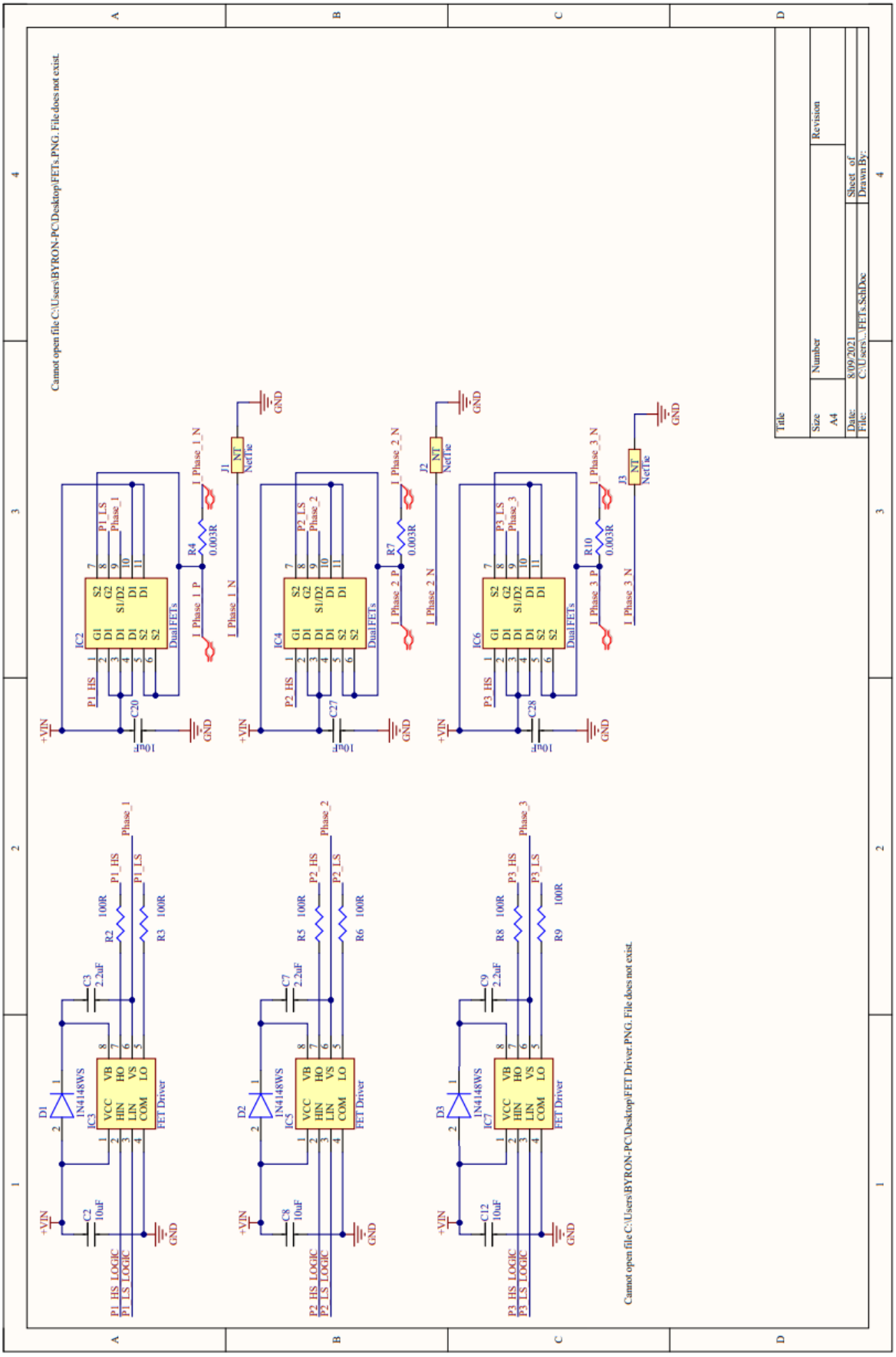

Fig. 19: MOSFETs and Drivers PCB Schematic

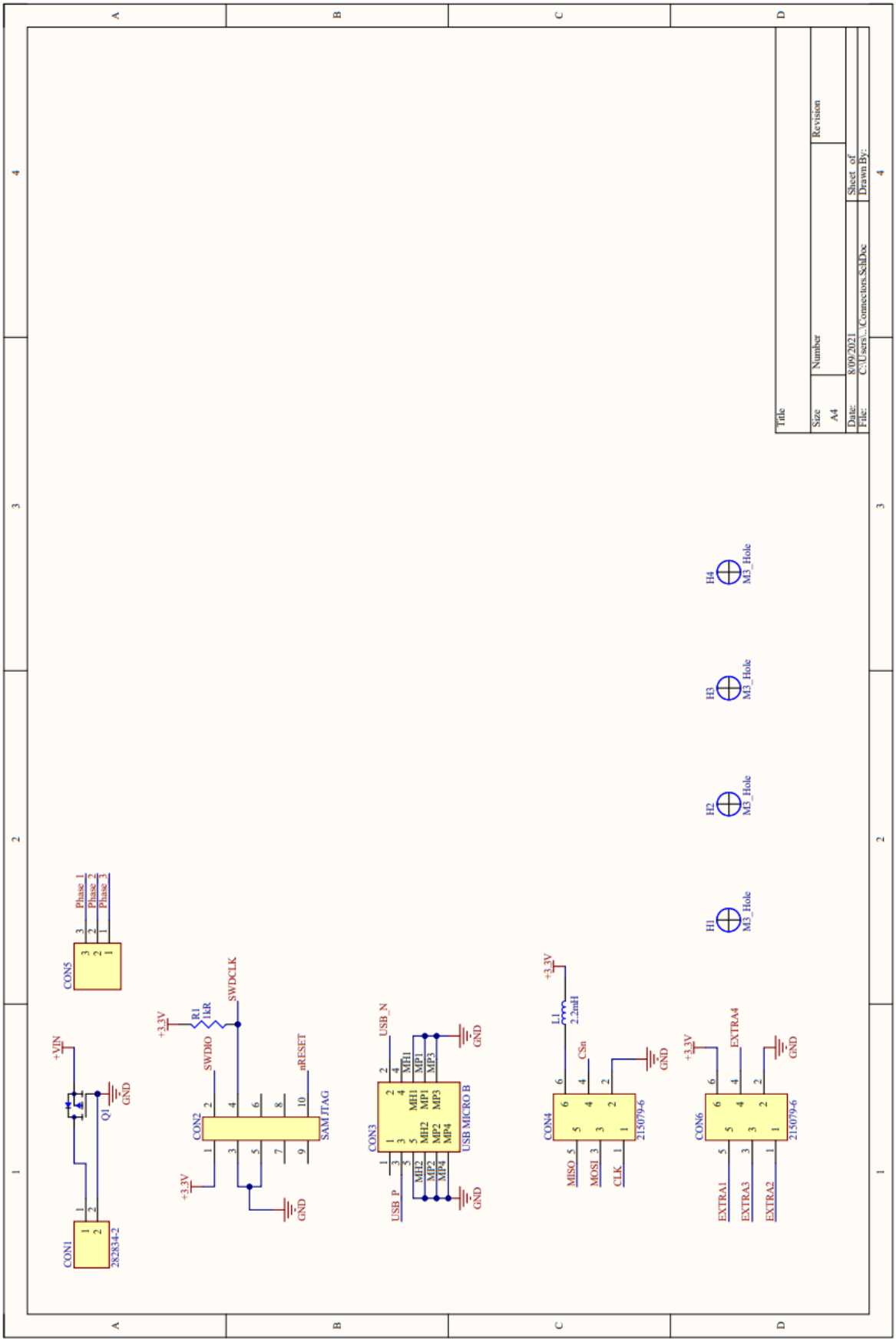

Fig. 20: Connectors and Mounting Holes PCB Schematic

6.12 Magnetic Encoder Schematics

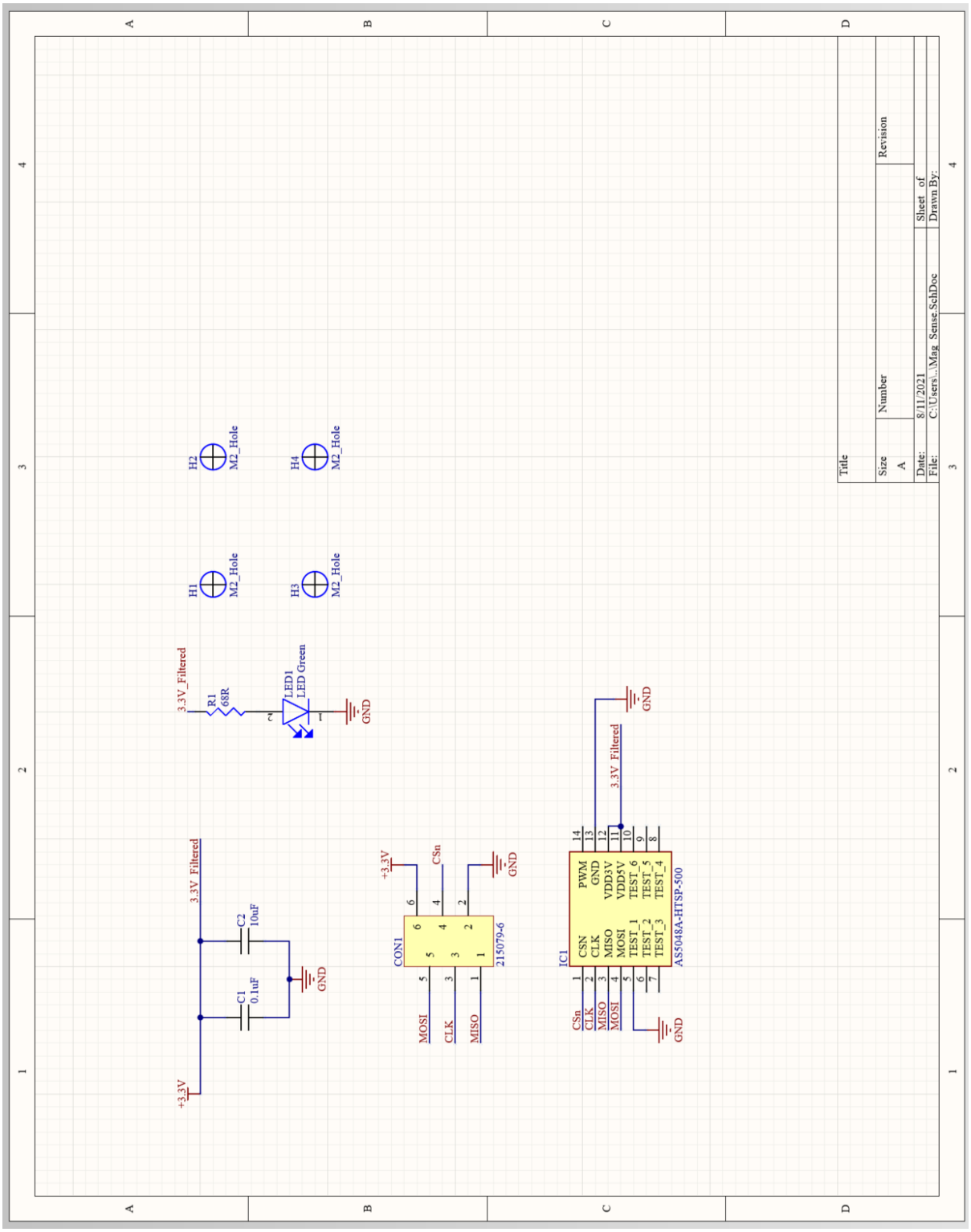

Fig. 21: Magnetic Encoder PCB Schematic

6.13 ESC PCB Board Views

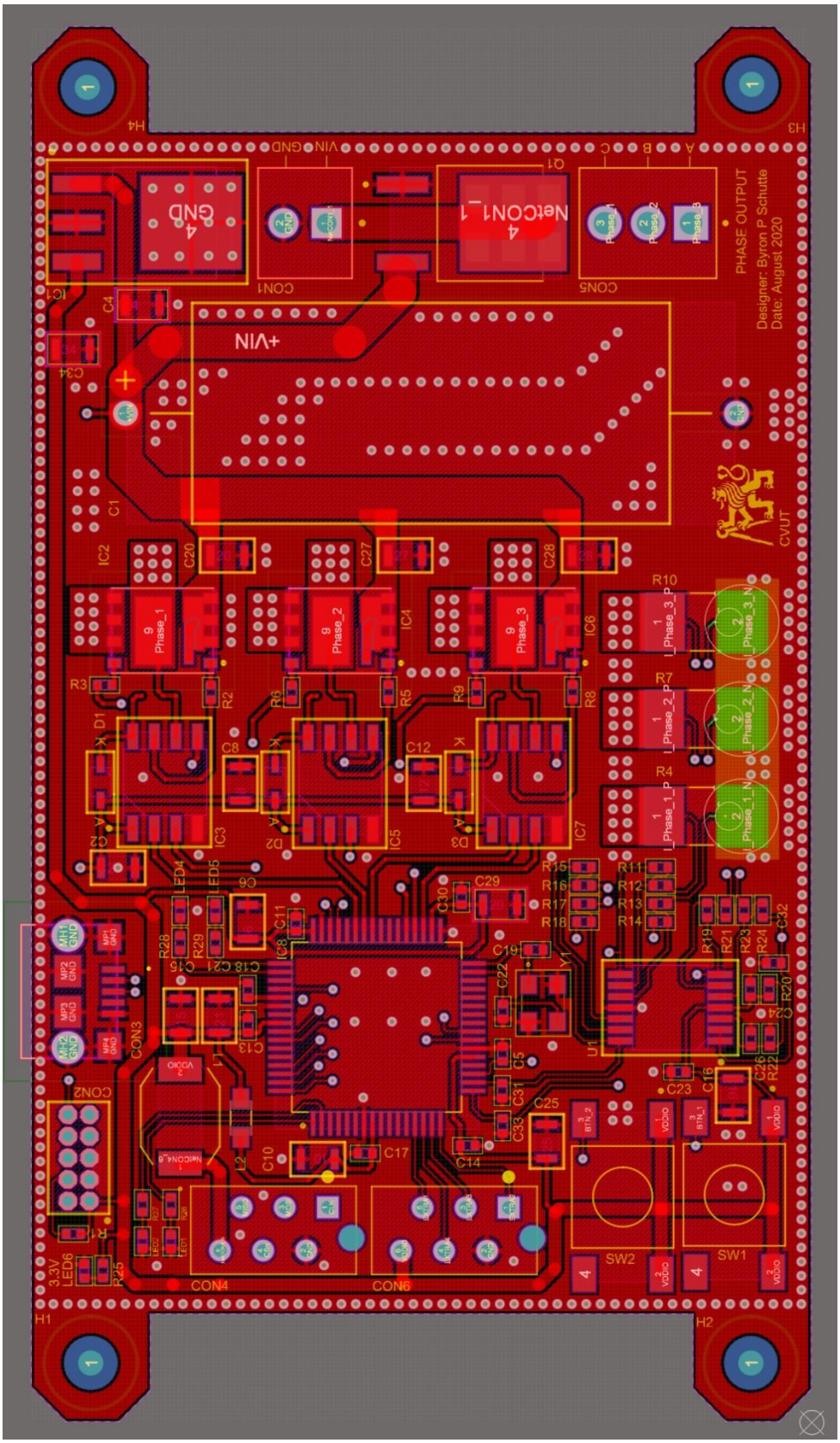

Fig. 22: Front Layer ESC PCB Board View

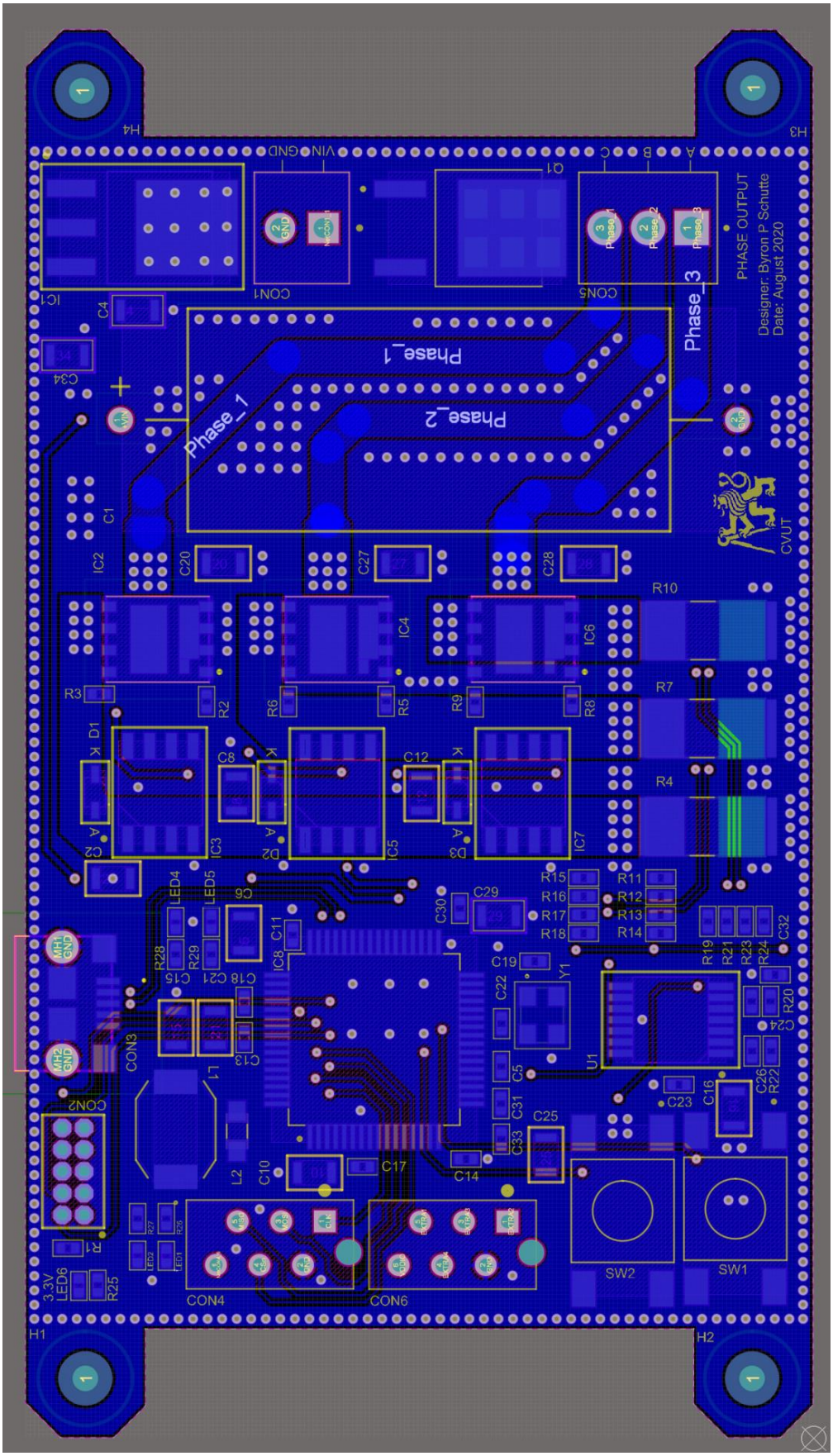

Fig. 23: Back Layer ESC PCB Board View

6.14 ESC PCB Assembly Diagram

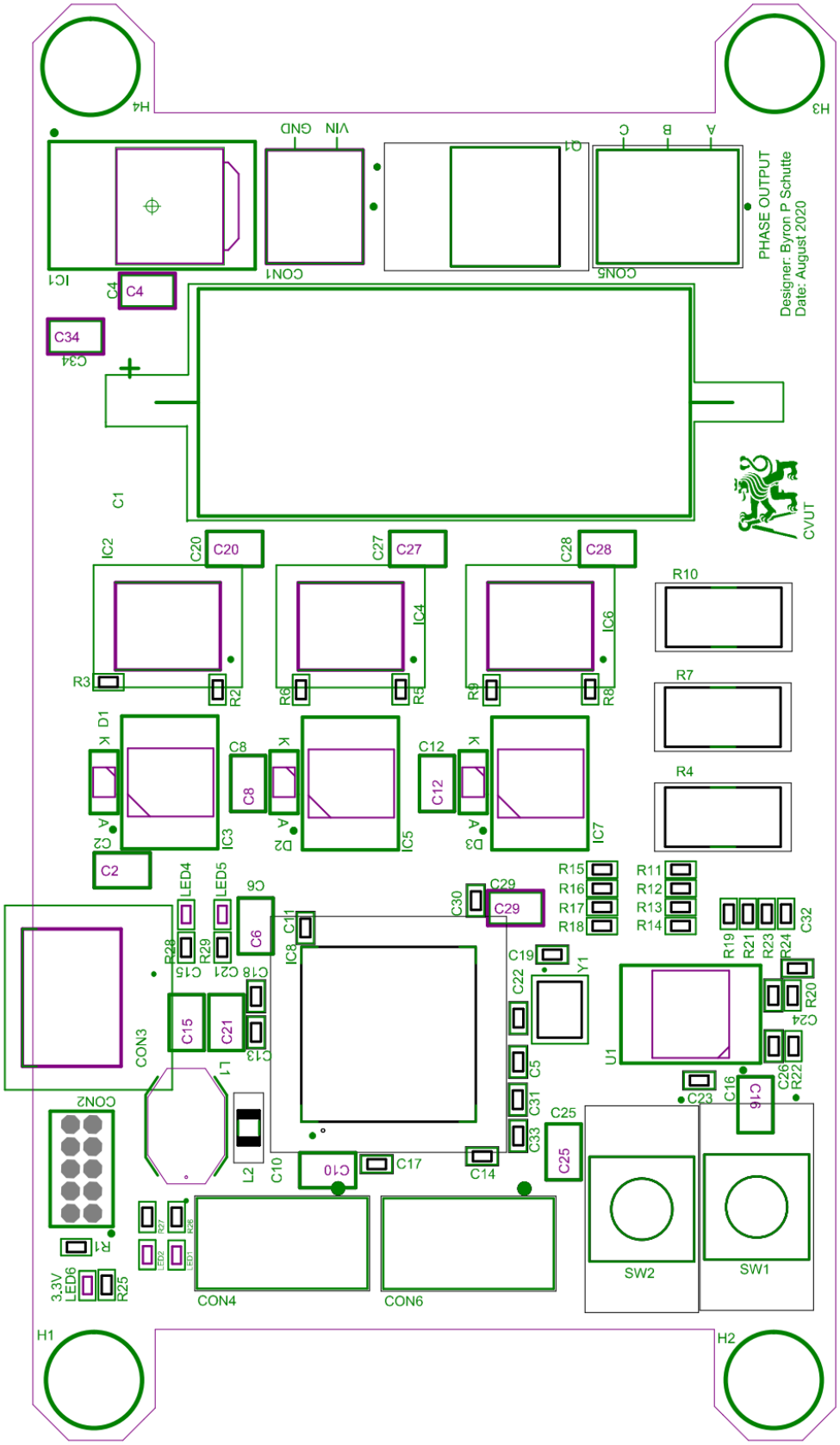

Fig. 24: ESC PCB Assembly Diagram

6.15 Magnetic Encoder PCB Board Views and Assembly Diagram

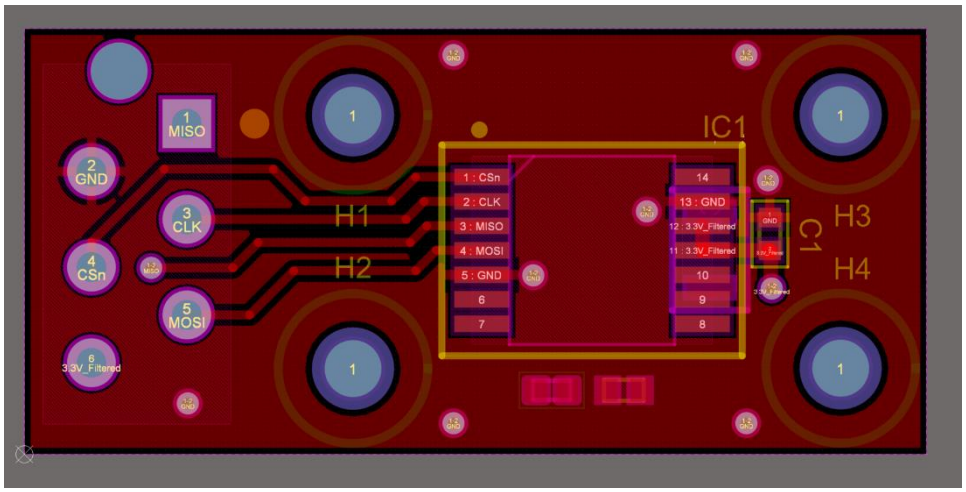

Fig. 26: Font Layer Magnetic Encoder PCB Board View

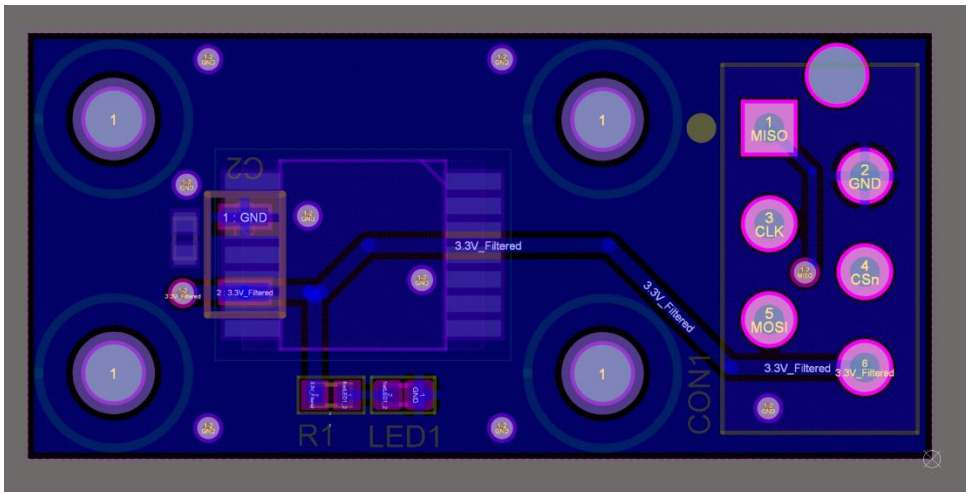

Fig. 27: Back Layer Magnetic Encoder PCB Board View

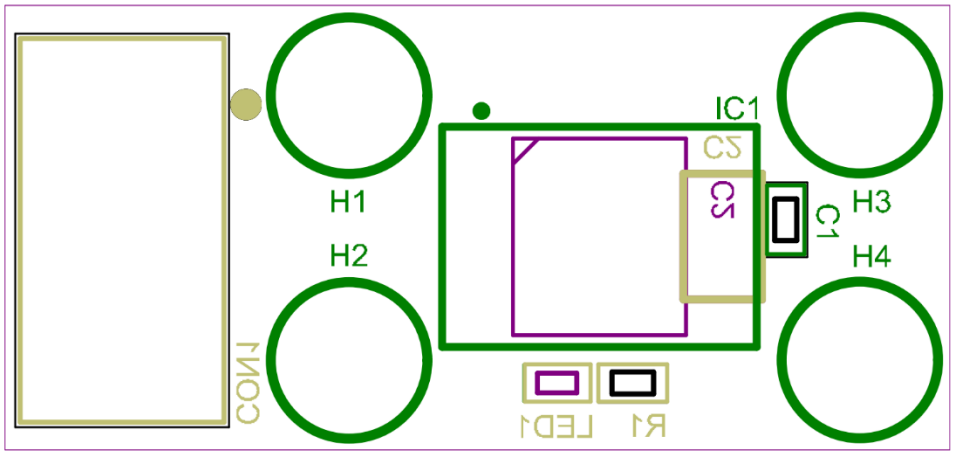

Fig. 25: Magnetic Encoder PCB Assembly Diagram

6.16 Bill of Materials

Manufacture ID	Description	Designator	Footprint	Quantity
MAL202117102E3	Capacitor 1000uF 40V 20%	C1	Capacitor Axial (12.5 X 30mm)	1
GMK212BBJ106KG-T	Capacitor 10uF 35VDC	C2, C4, C6, C8, C10, C12, C15, C16, C20, C21, C25, C27, C28, C29, C34	C0402	15
CGA2B2C0G1H101J050 BA	Capacitor 100pf 50V	C5, C31, C33	C0402	3
C1005X7R1H104K050B B	Capacitor 0.1uF 50V	C11, C13, C14, C17, C23, C24, C26, C30, C32	C0402	9
C1005X6S1C105K050B C	Capacitor 1uF 16V	C18	C0402	1
GJM1555C1H200FB01D	Capacitor 20pf 50V	C19, C22	C0402	2
282834-2	2P Screw Terminal	CON1	282834-2_1	1
20021111-00010T4LF	10P Male Connector	CON2	FCI_20021111-00010T4LF	1
10118193-0001LF	USB Micro B	CON3	101181930001LF	1
215079-6	6P Connector	CON4, CON6	THT 2.54mm	2
282834-3	3P Screw Terminal	CON5	TE_282834-3	1
1N4148WS	Diode	D1, D2, D3	SOD-323	3
M3_Hole	M3 Mounting Hole	H1, H2, H3, H4	M3_Hole	4
TLF80511TFV33ATMA1	3.3V LDO	IC1	TO252-3	1
BSC0921NDIATMA1	MOSFET (N-Channel)	IC2, IC4, IC6	TISON-8	3
IR2301SPBF	FET Drivers	IC3, IC5, IC7	SOIC-8	3
ATSAMD51J20A-MU	SAMD51 Microcontroller	IC8	QFP50P1200X1200X120-64N	1
SRR6603-222ML	2.2mH Inductor	L1	Inductor SRR6603-222ML	1
MLZ2012M150WTD25	15uH Inductor	L2	L0402	1
VLMG1500-GS08	Green LED	LED1, LED2, LED4, LED5, LED6	LED0402	5
IPD80P03P4L07ATMA1	MOSFET P-CH 30V 80A	Q1	TO252-3	1
CRCW04021K00FKEDH P	1K OHM 1% 1/5W 0402	R1, R12, R13, R16, R17, R21, R22, R23	R0402	8
RC0402JR-07100RL	100 OHM 5% 1/16W	R2, R3, R5, R6, R8, R9	R0402	6
CRE2512-FZ-R003E-2	0.003R, 2W, 1%	R4, R7, R10	R2512	3
CRCW040220K0FKED	20K OHM 1% 1/16W	R11, R14, R15, R18, R19, R24	R0402	6
RC0402FR-075K6L	5.6K OHM 1% 1/16W	R20	R0402	1
RC0402JR-07100RL	100 OHM 5% 1/16W	R25, R26, R27, R28, R29	R0402	5
SW_4-1437565-2	Push Button	SW1, SW2	SW_4-1437565-2	2
SOP65P640X120-14N	Quad OP Amp	U1	TSSOP-14	1
ABM8-12.000MHZ-20- B1U-T	12 MHz Crystal	Y1	OSC_Small_SC320X250X100N	1

Table 1: ESC Bill of Materials

Manufacture ID	Description	Designator	Footprint	Quantity
C1005X7R1H104K050 BB	0.1uF 50V	C1	0402	1
GMK212BBJ106KG-T	Capacitor 10uF 35VDC	C2,	0805	1
215079-6	6P Connector	CON1	THT 1.27mm	1
M2_Hole	M2 Hole	H1, H2, H3, H4	M2	1
AS5048A-HTSP-500	Magnetic Sensor	IC1	14-TSSOP	1
VLMG1500-GS08	Green LED	LED1	C0402	1
RC0402JR-07100RL	100R 1/16W	R1	0402	1

Table 2: Magnetic Encoder Bill of Materials

7 Software Implementation

7.1 Sinusoidal PWM

This block generates sinusoidal voltages that will be modulated across the motor. The block takes in the following parameters

- Electric angle which is measured by the rotary encoder or estimated by the observer
- Desired Direct Voltage
- Desired Quadrature Voltage

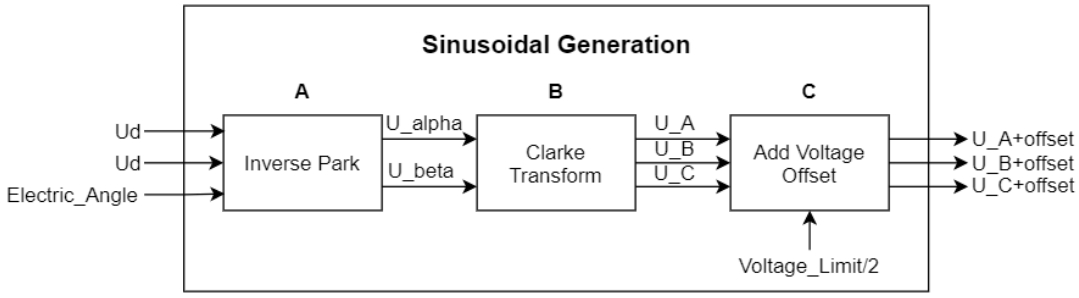

Fig. 28: Sinusoidal Generation Block Diagram

The Following happens in each block.

A. The Inverse park (Eq 4) is computed and the U_α and U_β values are now generated
B. The Clarke transforms (Eq 5) is computed and the U_α and U_β voltages are converted to U_A, U_B and U_C phase voltages
C. An offset voltage is added the phase voltages since the inverter cannot supply negative voltages, therefor 0 will correspond to half the maximum allowed voltage.

7.2 Phase Voltage Generation

This block takes in 3 parameters which are the desired phase voltages. The voltages are checked if they are within the limits, they are converted to duty cycles and are written to the hardware counters in the time compare registers.

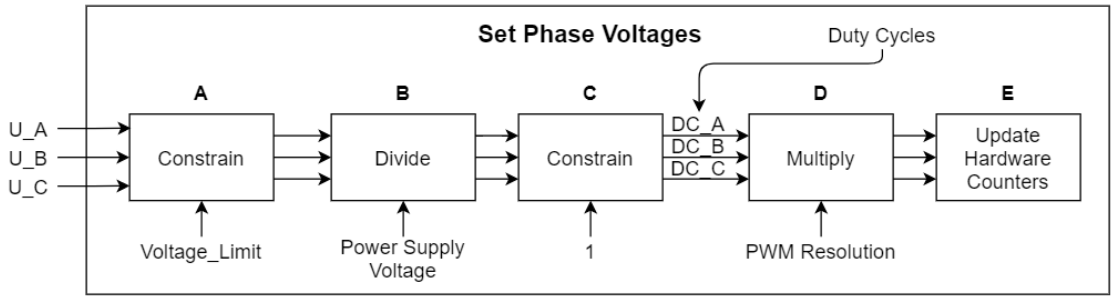

Fig. 29: Set Phase Voltages Block Diagram

A. The desired phase voltages are constrained within the range $[0, \text{voltage\_limit}]$
B. The desired phase voltages are now divided by the actual supply voltage (Eq2) resulting in a value within the range $[0,1]$
C. The results from block B are again constrained within the range $[0,1]$, the duty cycles are now calculated.
D. The duty cycles are now converted to timer domain values by multiplying the duty cycles to the PWM resolution.
E. The duty cycles in the timer domain are written to the hardware register of the TCC counter.

7.3 Current Capture

The TCC Interrupt block is executed every time the counter reaches zero, all low side switches will be active at this point. The ADC is then triggered to capture the voltages at the current shunts. The raw values are converted to voltages. The DC offset and Gain is removed, the voltage is then converted to current using Eq. 17. The interrupt flag is lowered and the function returns.

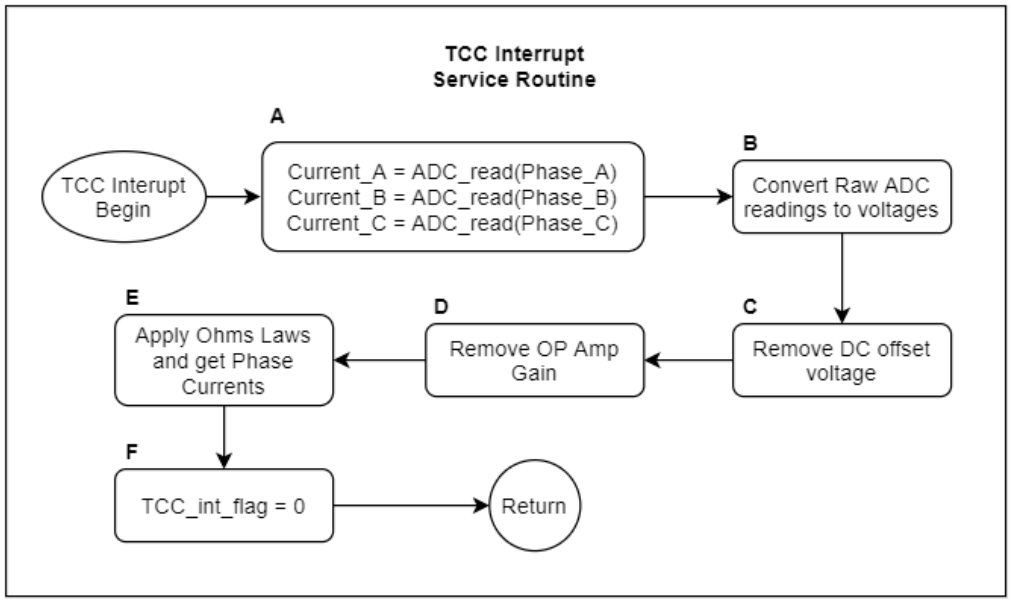

Fig. 30: Timer Interrupt Handler Block Diagram

A. The currents are received from the ADC.
B. The raw values are converted to voltages.
C. The DC offset is removed
D. The gain is removed.
E. Ohms law is applied, and the currents are solved.
F. The Interrupt Flag is lowered.

7.4 Field Orientated Controls Currents

This block converts the captured currents into the $\alpha\beta$ frame using the Clarke Transform using Eq.6. Once the currents are converted, they are stored in a global variable.

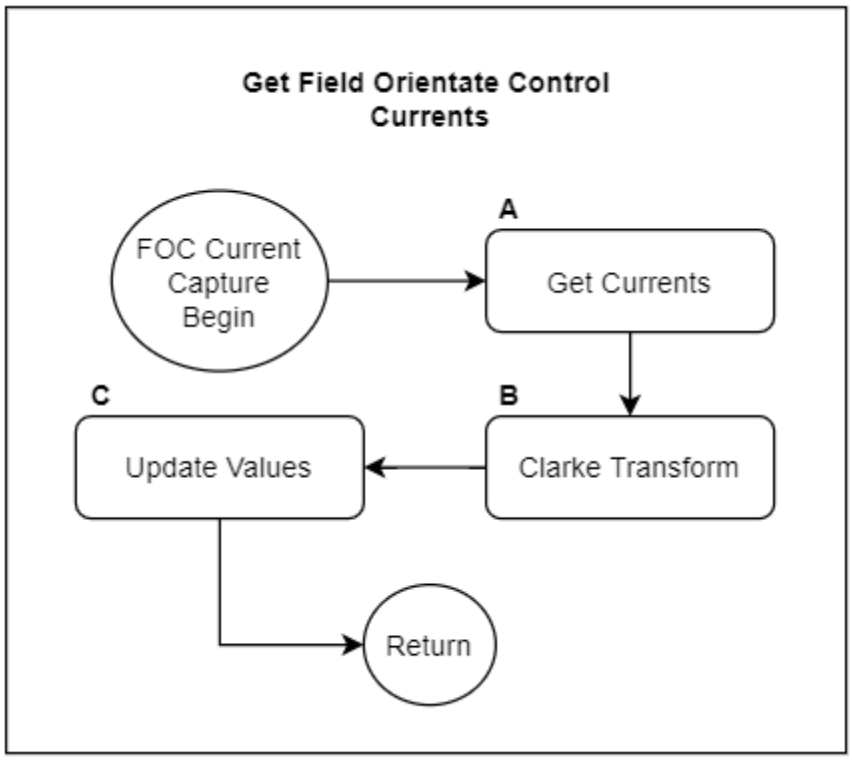

Fig. 31: Field Orientated Control Current Block Diagram

A. The currents are fetched from the global variables
B. The Clarke transform is applied
C. The converted currents are stored in global variables.

7.5 Angle Encoder Capture

The Angle Encoder function is called when the FOC function need the rotors angle. The angle is received via the SPI interface, the angle is received in a 14 bit raw value. The new angle is compared to the old value, if the difference is greater than 10% of the full value, this indicates that one revolution has been made. The full revolutions are recorded in a global "full rotation" variable, once the new angle has been converted from binary to radians the full rotations are added to the result.

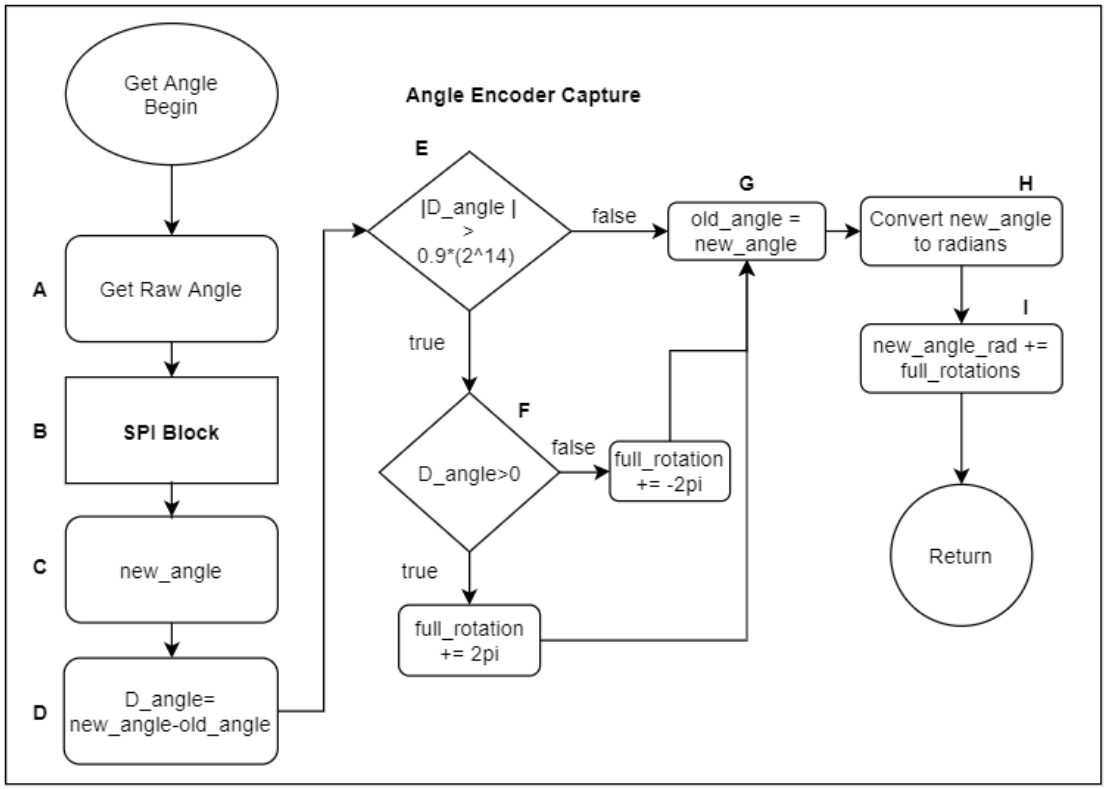

Fig. 32: Angle Encoder Capture Block Diagram

A. The Raw angle command is fetched
B. The command is pushed into the SPI block
C. The new angle is received
D. The difference between the new and old angle is calculate
E. If the absolute value of the difference in angles is greater than 90% of the full scale of the magnetic encoder, then go to F else go to G
F. If the full rotation was made in a positive direction add $[2\pi]$ else add $[-2\pi]$
G. Update old angle variable
H. Convert the raw angle into radians
I. Add full rotations to the new angle

7.5.1 SPI Block

The SPI block oversees sending commands to the magnetic encoder and receiving the response. Depending on the command being sent the read bit will either be high or low, an OR operation is then done to the command and the read bit. The parity is calculated and joined to the command byte. Once the command is sent the program will await a response from the hardware block. If the error bit is high from incoming data the global error flag will be raised. The error and parity bit are then removed and the 14bit angle data will be passed to the Angle Encoder Block.

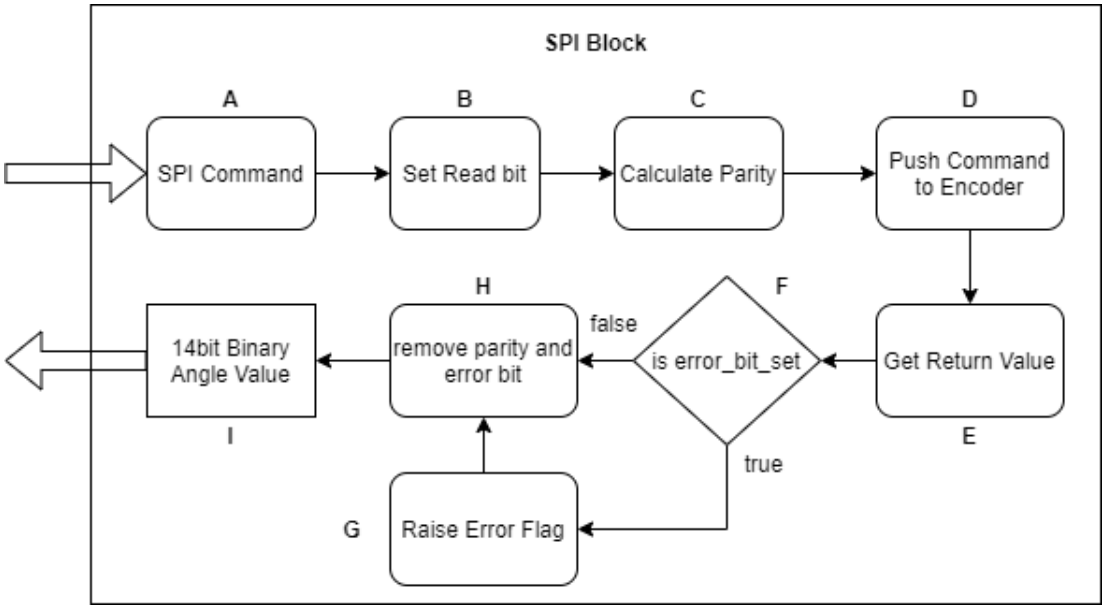

Fig. 33: SPI Block Diagram

A. The Command is received
B. The read bit is joined to the command
C. The parity bit is calculated and joined to the command
D. The Command is pushed to the SPI hardware block
E. The response is captured
F. The error bit is checked
G. If the error bit is set, the global error flag is raised
H. The error and parity bit are removed
I. The data is returned to the calling function

7.6 State Observer

The State Observer will estimate the angle of the rotor by taking in U_α and U_β from the modulation block and I_α and I_β from the measured currents. The phase resistance, phase inductance, observer gain, and flux linkage values are also given. The estimated angle is then fed into the angle selector block where the program will either take the value from the encoder or the observer (Eq 12).

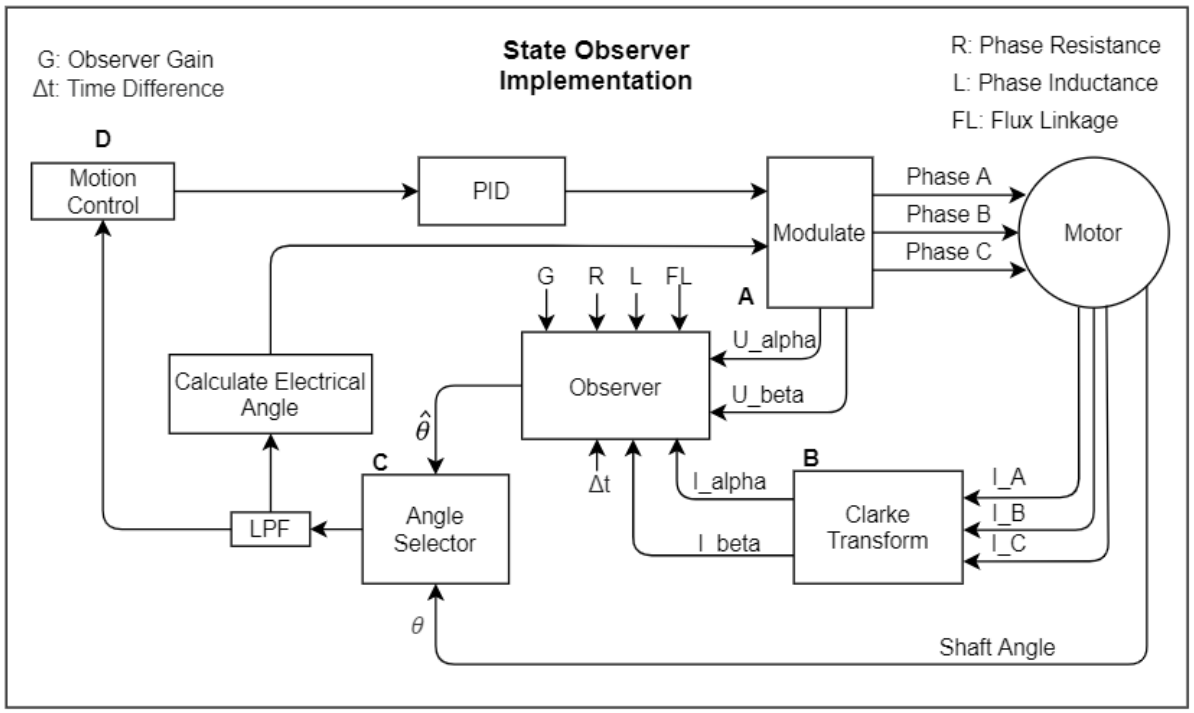

Fig. 34: State Observer Implementation Block Diagram

A. The modulated voltages U_α and U_β are passed into the Observer
B. The currents generated from U_α and U_β are read and converted into the same reference frame (I_α and I_β) and then fed into the observer
C. The angle from the observer and the encoder are passed into the angle selector, depending on the sensing mode either angle will be passed in the control loop
D. The control loop handles the given angle and performs the necessary task.

7.7 Angle Closed Loop

The Angle Closed Loop function will attempt get the shaft angle to the desired value which has been set by the user. The actual angle is received from the encoder or the observer, the electrical angle is calculated. The difference between the desired and actual angle is calculated. This difference is the error. The error is fed into a PID control loop which will generate the necessary output to get the error to zero.

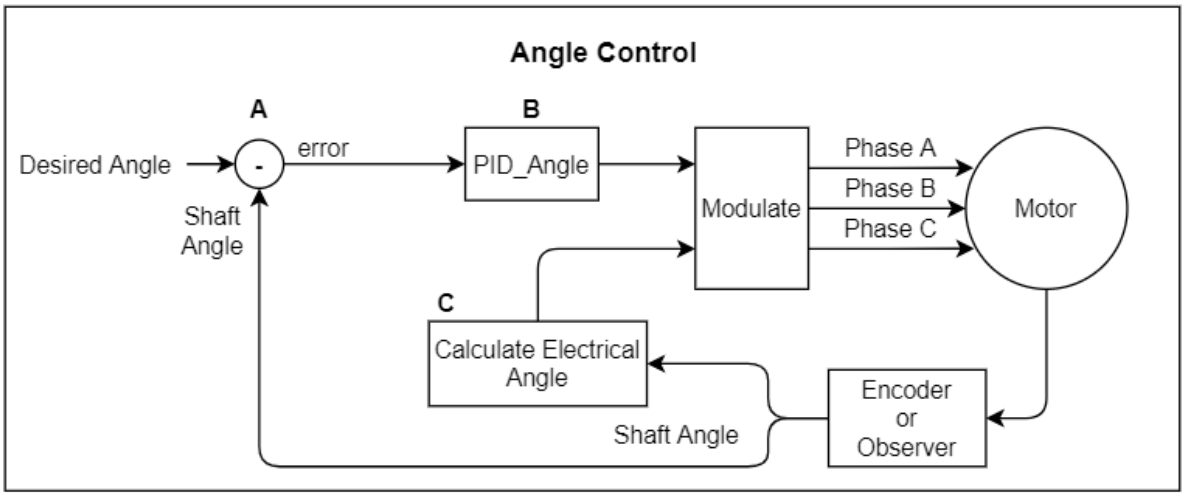

Fig. 35: Angle Control Block Diagram

A. The error is calculated by subtracting the shaft angle from the desired angle
B. The error is fed into the Angle PID loop and the compensation is fed into the modulation block
C. The electrical angle is calculated and passed into the modulation block

7.8 Velocity Closed Loop

The Velocity Closed Loop function will attempt to get the motors shaft to rotate at a constant velocity that has been set by the user. The actual angle is received from the encoder or the observer, the velocity of the motor is calculated based off the previous and current angle, and the time elapsed between the readings. The calculated velocity is fed into a low pass filter which will suppress any large changes in velocity which are consider noise. The filtered velocity is subtracted from the desired velocity and the error is fed into a PID loop.

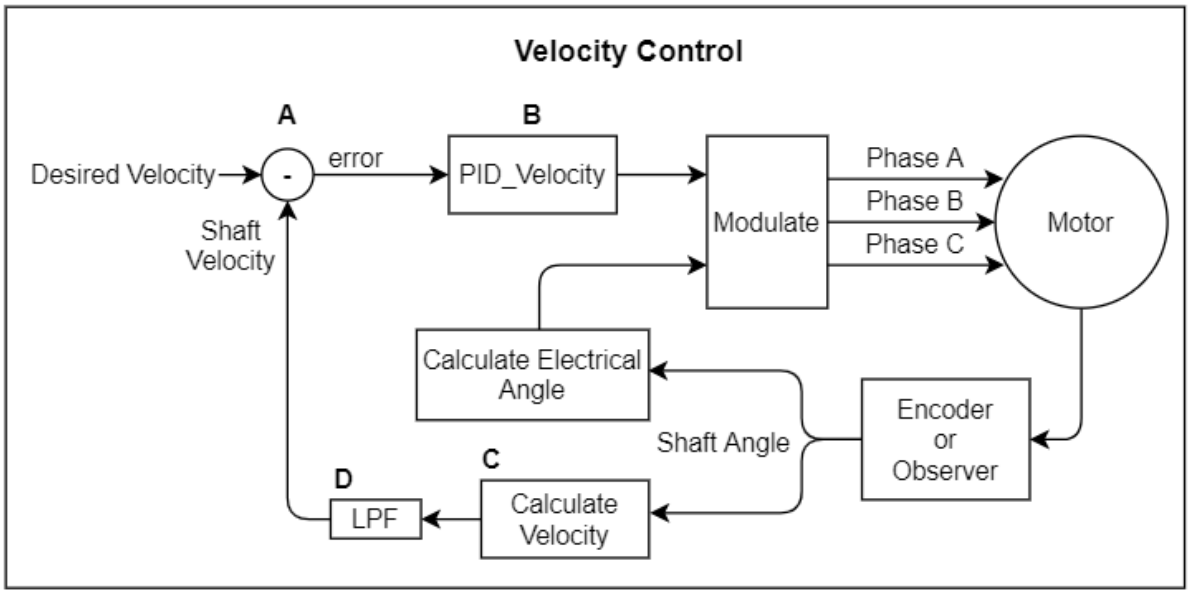

Fig. 36: Velocity Control Block Diagram

A. The error is calculated by subtracting the velocity from the desired velocity
B. The error is fed into the velocity PID loop and the compensation is fed into the modulation block
C. The velocity is calculated based off the new angle
D. The new velocity is fed into the LPF to suppress any noise in the velocity

8 Results

8.1 Current Capture

The following figures were captured from the ESC while operating in a constant velocity mode at 5 rad/sec. In Fig. 37 the current measured on phase A was plotted. The motor was running with no mechanical load, the wave form appears noisy, but a sinusoidal signal is visible. In Fig. 38, a mechanical load was place on the motor, this increased the consumed current. The wave form is clear with minimal noise. In Fig 39 all three phases are plotted, no load was present on the motor. The same noise is apparent as seen in Fig. 38. In Fig 40 all phase currents were plotted while a mechanical load was present. The amplitudes of the currents are greater, and the waveforms are clear with minimal noise. The waveforms are phase shifted by 120 degrees. In Fig. 41 the modulated voltage and its respective current were plotted. Both waveforms were in phase.

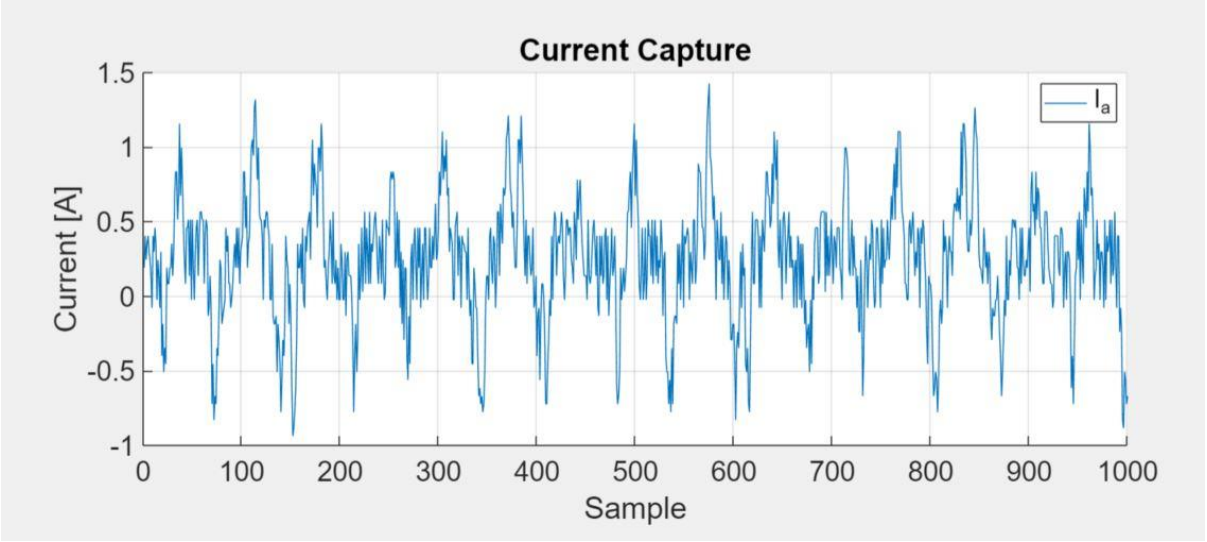

Fig. 38: Single Phase Current with no Mechanical Load

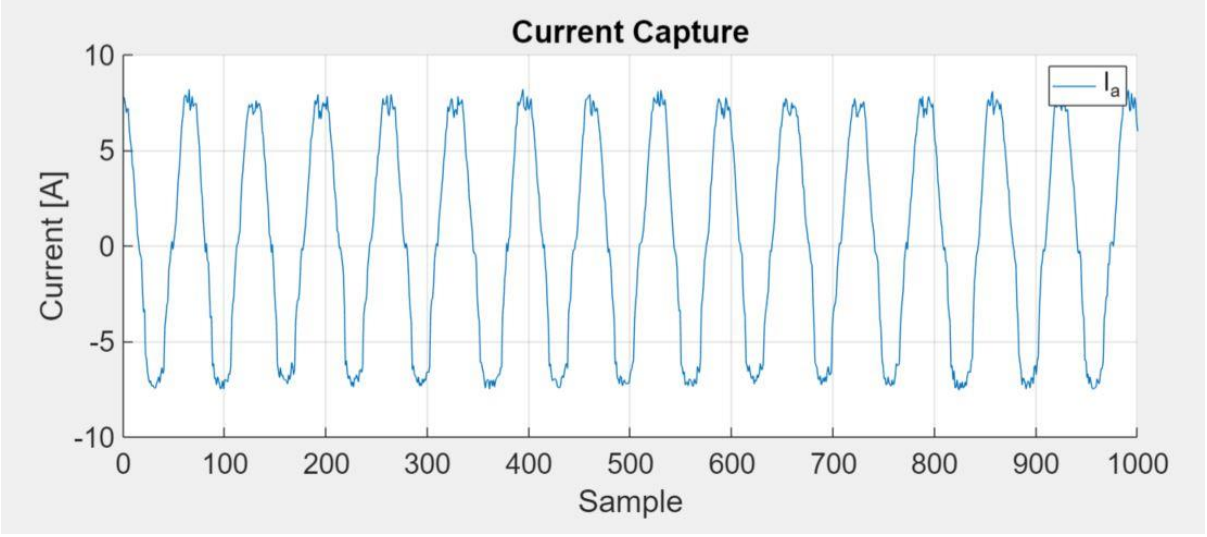

Fig. 37: Single Phase with Mechanical Load

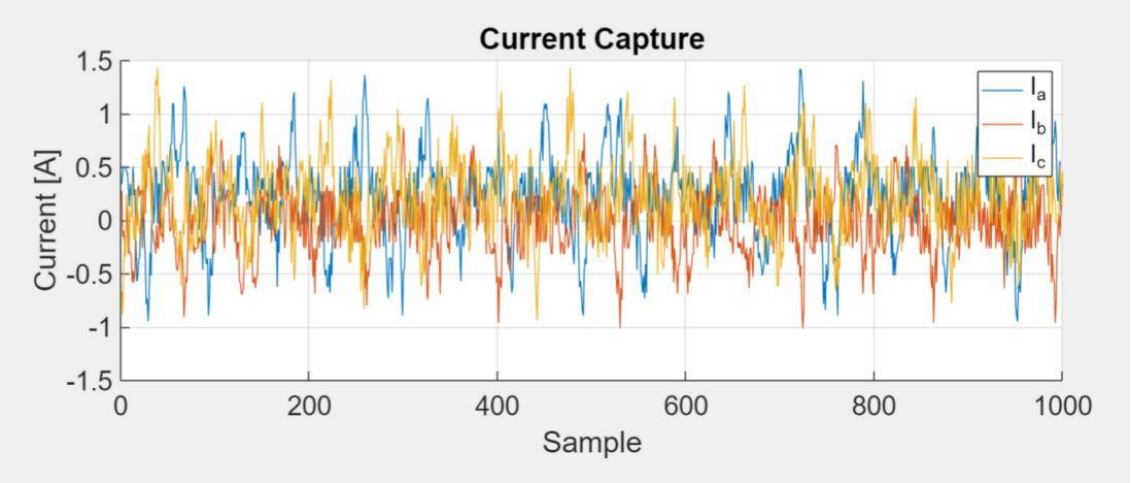

Fig. 39: Three Phase Currents with no Mechanical Load

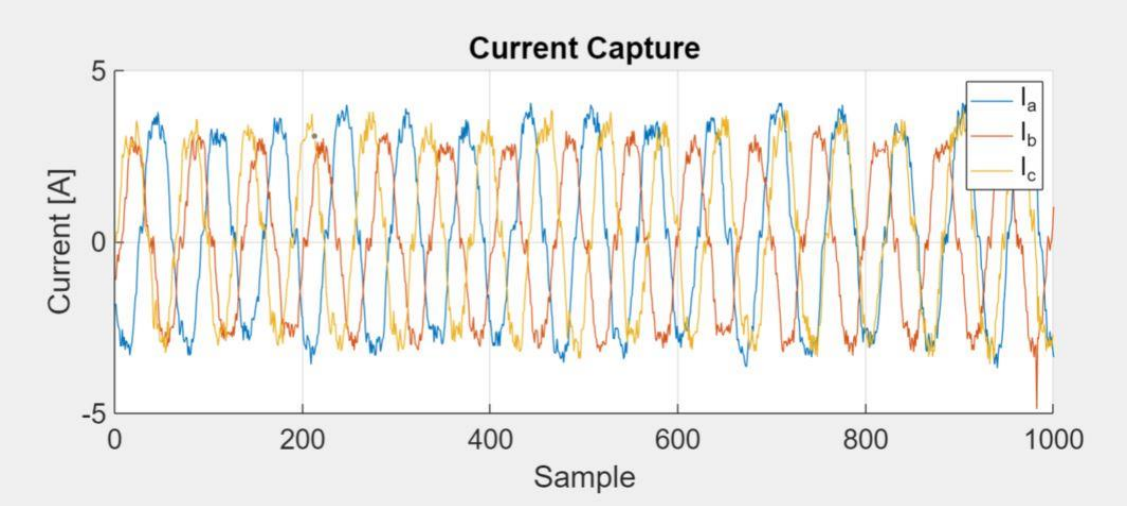

Fig. 40: Three Phase Currents with Mechanical Load

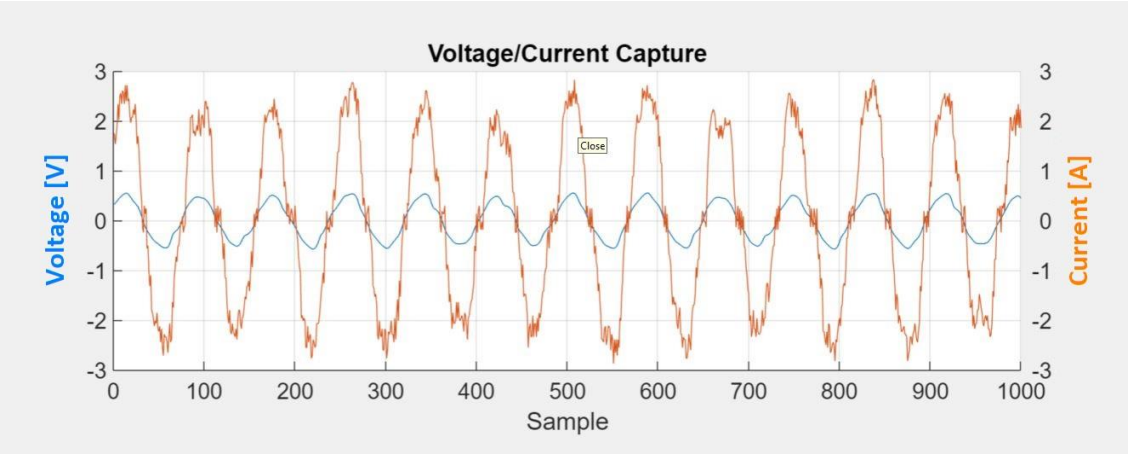

Fig. 41: Voltage and Current Waveforms

8.2 Velocity Closed Loop

The following figures were captured from the ESC while operating in a constant velocity. In Fig. xx the velocity was set to 5 rad/sec. The measured velocity was fluctuating between 20 and -10 rad/sec. The mean value was centered near 5 rad/sec. In Fig. xx the set velocity was 100 [rad/sec]. The measured velocity was fluctuating between 150 and 0 rad/sec, the mean value was centered just below 100 rad/sec. The noise from the measured velocity was quite severe, a Low Pass Filter was placed on the output of the function but did not limit that large changes. The actual velocity observed on the shaft was constant.

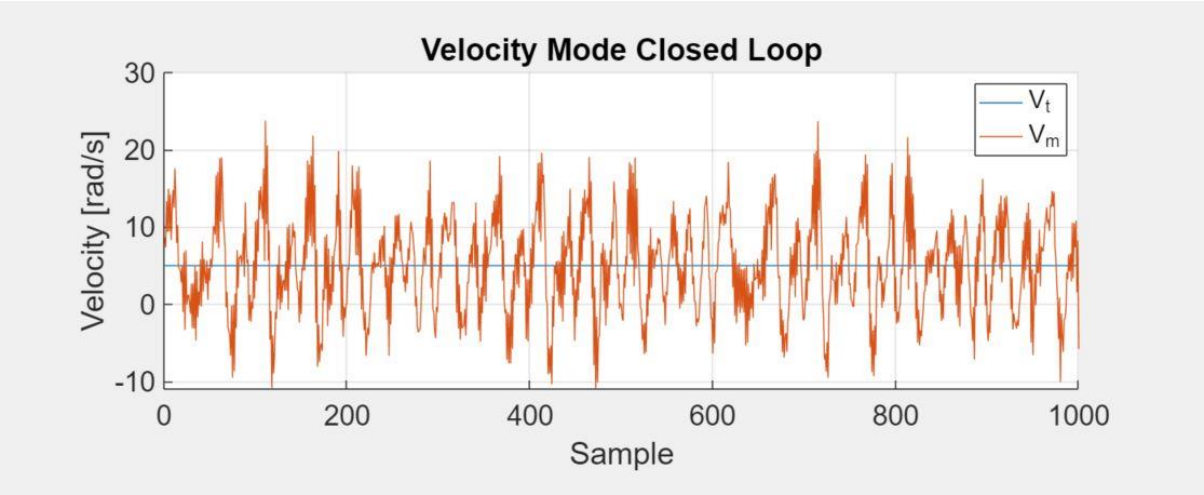

Fig 42: Measured Velocity at 5 rad/sec

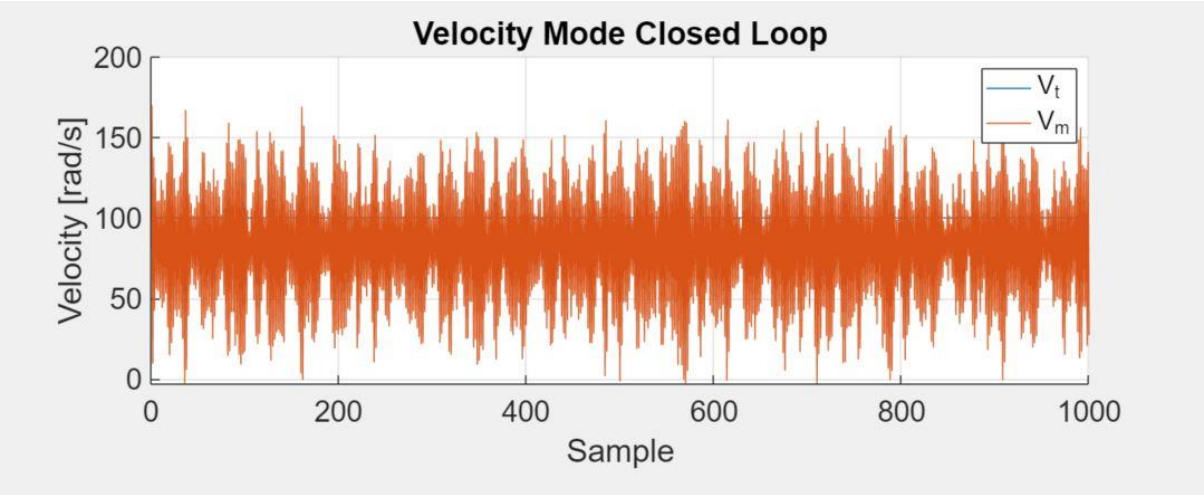

Fig 43: Measured Velocity at 100 rad/sec

8.3 Angle Closed Loop

The following figures demonstrate the angle closed loop functionality. In Fig. 44 the set angle is 5 rad. The motor shaft was mechanically displaced in both directions, the shaft returned its set point with slight over and undershoots. In Fig 45 the set angle was flipping between 6 rad 0 rad. The shaft was stable at both set angles, the shaft was able to reach the set position with slight over and undershoots.

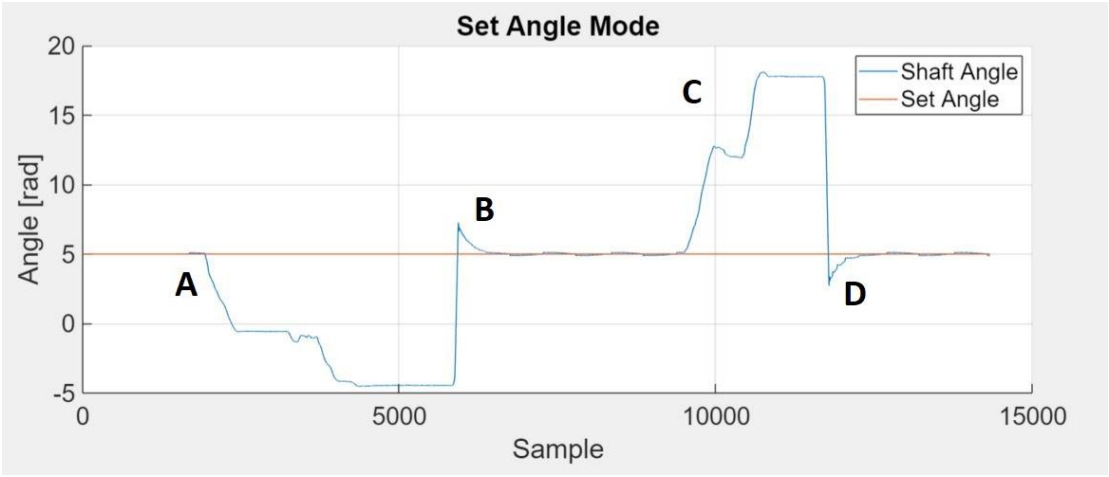

Fig 44: Set Angle Displacement

A. The shaft is displaced 5 rad in a negative direction
B. The shaft is released, an overshoot occurs.
C. The shaft is displaced 15 rad in the positive direction.
D. The shaft is released, an undershoot occurs.

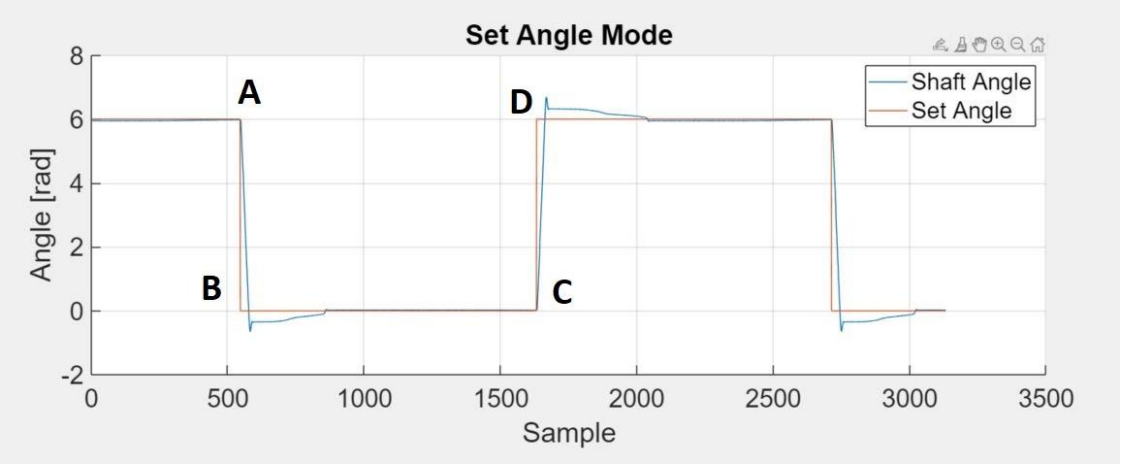

Fig 45: Flipped Set Angle Behavior

A. The set point changes from 6 rad to 0 rad
B. The shaft moves to the new set point, an undershoot occurs.
C. The set point changes from 0 rad to 5 rad
D. The shaft moves to the new set point, an overshoot occurs.

8.4 Angular Estimation with Sate Observer

The state observer was first implemented in MATLAB. U_α,U_β, I_α and I_β were passed into MATLAB via the USB interface in buffered packets. In Fig. 46 the voltages and currents are plotted together while no load was present on the shaft. Sinusoidal waveforms were present but the noise in the currents severe. In Fig. 47 a mechanical load was applied to the shaft. The currents were an order of magnitude larger than Fig 46. The noise was less severe. The voltages and currents were in phase.

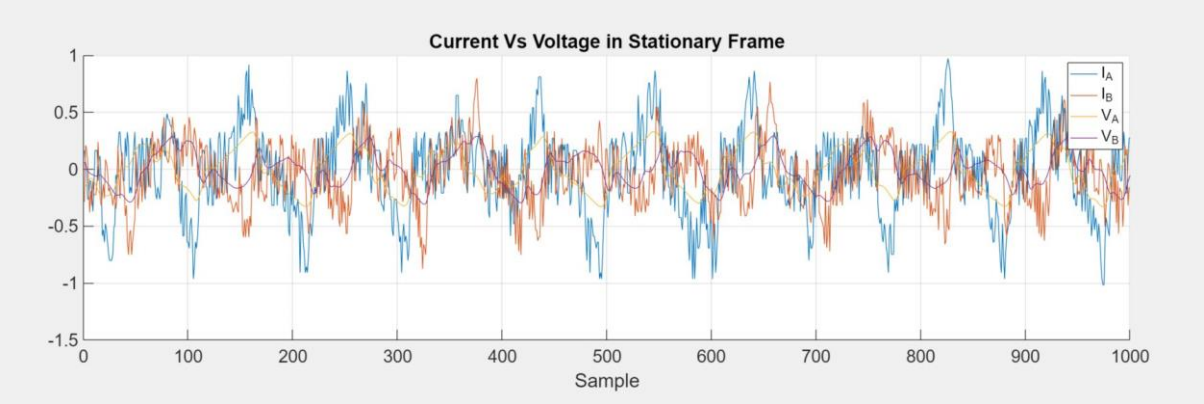

Fig 46: Alpha/Beta Current and Voltages with no Load

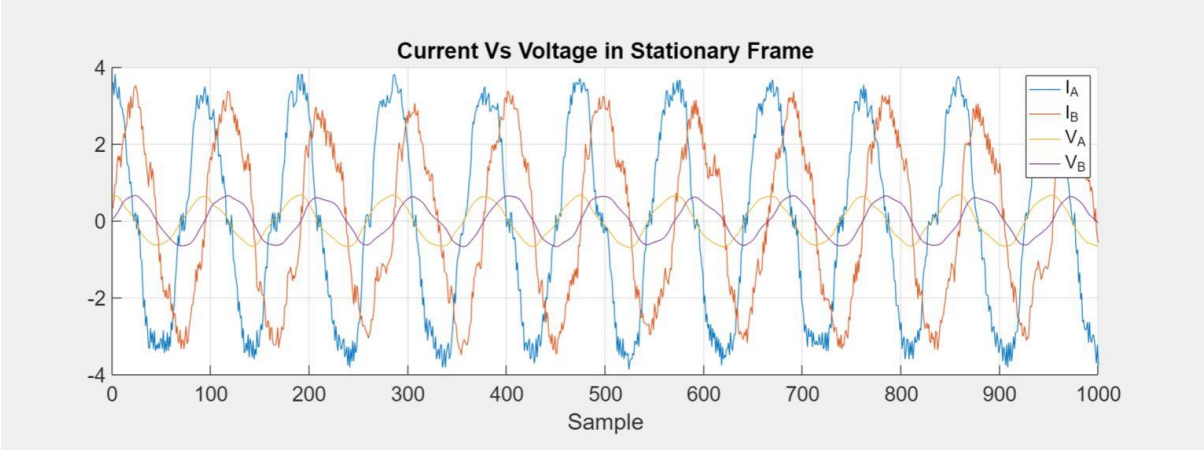

Fig 47: Alpha/Beta Current and Voltages with a Load

Once the observer was implemented in MATLAB the stator flux vectors and estimated angle were plotted fig. 48. No reference angle was used at this point. Tunning the observer was priority. The following operating parameters were found to keep the observer stable.

$$ObserverGain: 5000[-],$$
$$FluxLinkage: 0.004[Wb].$$

The properties of the motor were measured with a "Multi-function Tester – TC1"

$$StatorInductance: L_s = 0.02[mH],$$
$$Stator\ Resitance: R_s = 1.6\ [\Omega].$$

The observer was then implemented in C with the same operating parameters found in MATLAB. In Fig. 49 the motor was spinning with no load. The measured angle and estimated angle are plotted together. Although the maximum and minimum values are in phase, the amplitude was small. In fix 50 a load was applied to the motor. The estimated angle now matched the measured angle in phase and amplitude.

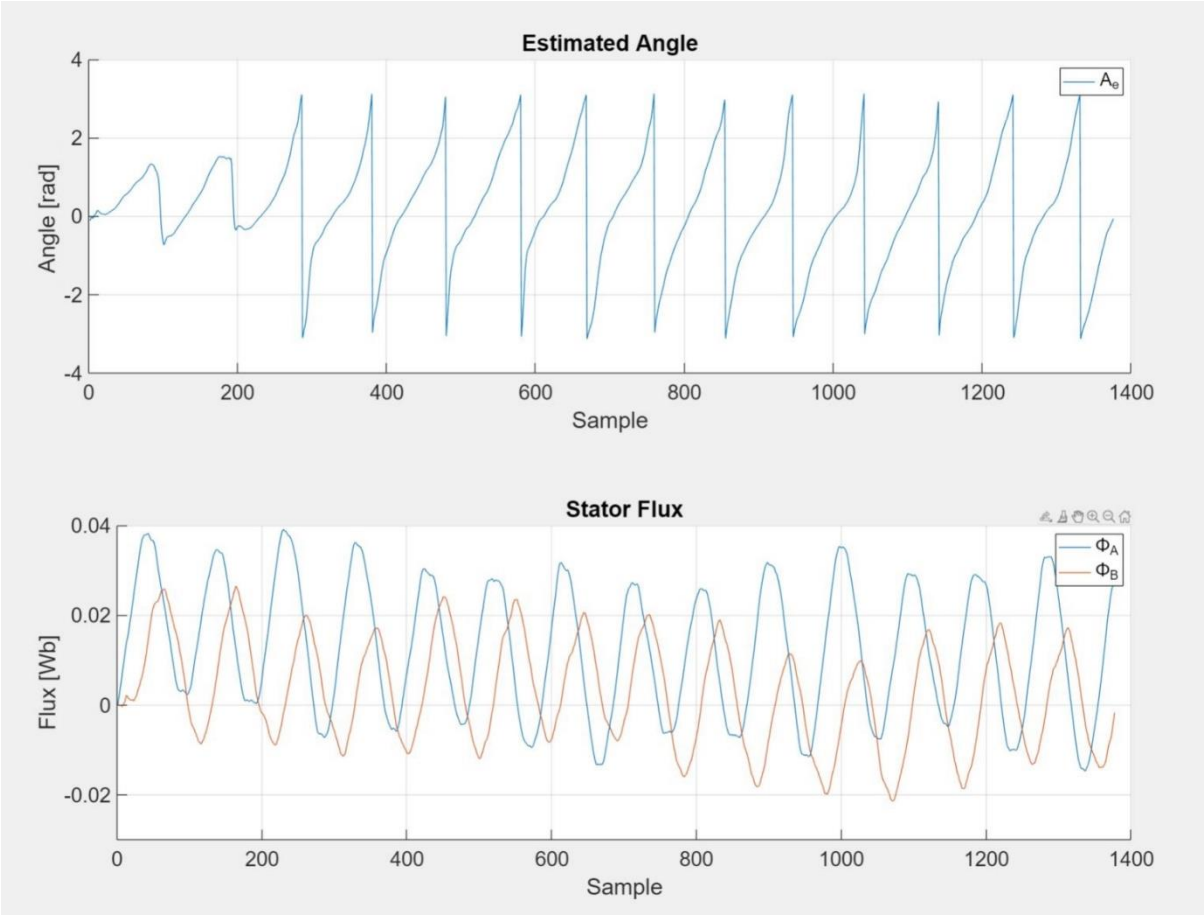

Fig 48: Estimated Angle and Stator Flux in MATLAB

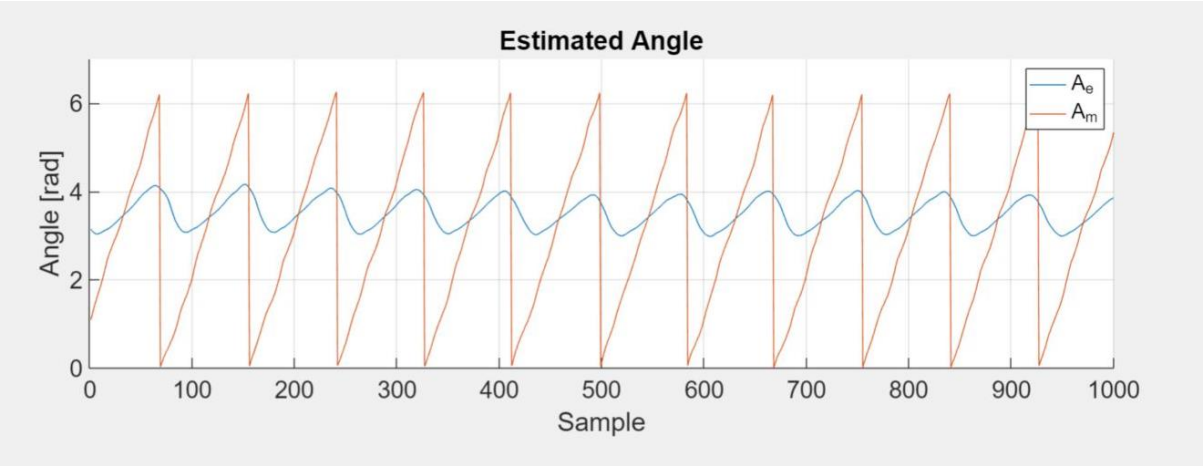

Fig 49: Estimated Angle in C Code with No Load

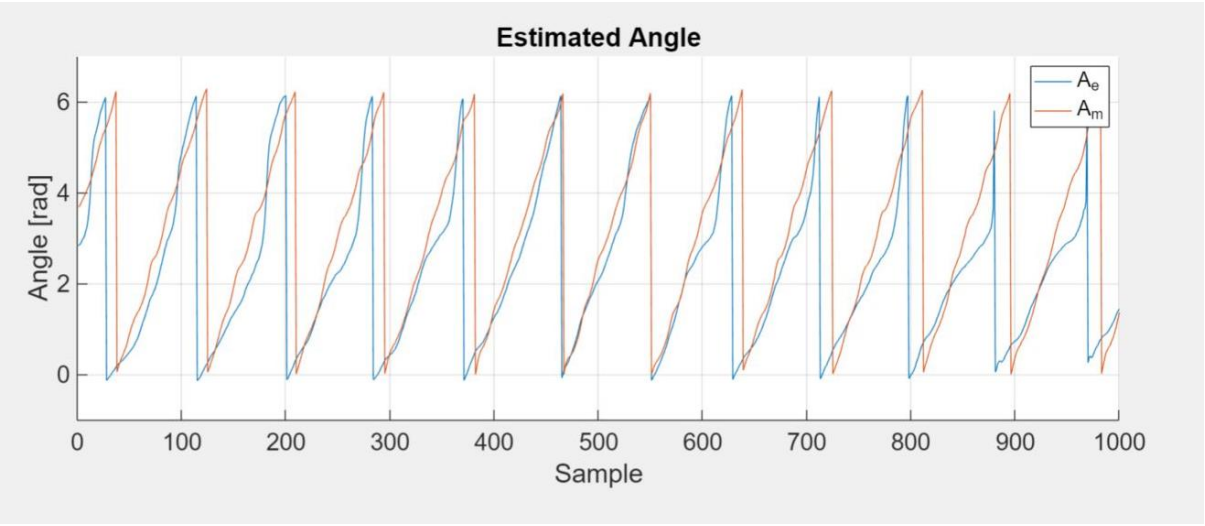

Fig 50: Estimated Angle in C Code with Load

9 Conclusion

An Electric Speed Controller was designed in Altium Designer. A motor mount was 3D printed that coupled the BLDC motor to a magnetic. A magnetic encoder was mounted behind the motor for angular measurements. Low side current sensing was implemented for sensor-less control. Field orientated control was implemented in C and basic motion control such as desired angle and velocity was achieved. A state observer was implemented to estimate the angle of the motor shaft using voltages/currents in the rotating reference frame. Estimating the shaft of the angle was possible but was not stable. The state observer would saturate due to noise in the current measurements, therefor to keep the estimated angle stable a load needed to be applied to the motor to push the currents out of the noise floor. Switching the ADC reference voltage to the internal band gap voltage reference could reduce the noise. Triggering the ADC with hardware interrupts could speed up current readings. The flux linkage of the motor was estimated. Using a measured value could help with tuning the observer.

10 References

1. Solbakkenspace, Y. *"Vector PWM Intro,"* 2019. Available at: https://www.switchcraft.org/learning/2017/3/15/space-vectorpwm-intro.
2. Cakanel, Ahmet & Vadim, I & Utkin, Vadim. *"Frequency Control of DC/AC Inverter,"* 2016. Available at: https://www.researchgate.net/figure/Circuit-Diagram-of-Three-Phase-Inverter-and-Load_fig1_311047927.
3. Maximintegrated.com, "*Reverse-Current Circuitry Protection,"* 2021. Available at: https://www.maximintegrated.com/en/design/technical-documents/app-notes/6/636.html.
4. toshiba.semicon-storage.com, *"Basics of Low-Dropout (LDO) Regulator ICs,"* 2021. Available at: https://toshiba.semicon-storage.com/info/docget.jsp?did=13766.
5. Zhao, J. and Yu, Y., *"Brushless DC Motor Fundamentals, "* 2014. Available at: https://www.monolithicpower.com/pub/media/document/Brushless_DC_Motor_Fundamentals.pdf.
6. Grandviewresearch.com, "*Global Brushless DC Motor Market Size Report, 2021-2028,"* 2021. Available at: https://www.grandviewresearch.com/industry-analysis/brushless-dc-motors-market.
7. microchip.com, *"Using PWM to Generate an Analog Output,"* 2020. Available at: http://ww1.microchip.com/downloads/en/Appnotes/90003250A.pdf.
8. Havanur, S, "*Matching System Dead Time to MOSFET Parameters in ZVS Circuits,"* 2014. https://www.vishay.com/docs/67527/matchingsystemdeadtime.pdf.
9. Duane C. Hanselman, *"Brushless Permanent Magnet Motor Design,"* Lebanon, Magna Physics Publishing, second edition, 2003.
10. Ams.com, *"AS5048A/AS5048B Datasheet,"* 2018. Available at: https://ams.com/documents/20143/36005/AS5048_DS000298_4-00.pdf.
11. Skuric, A, "*Arduino Simple Field Oriented Control (FOC) project,"* 2021, Available at: https://docs.simplefoc.com.
12. Lee, J., Hong, J., Nam, K., Ortega, R., Praly, L. and Astolfi, A, "*Sensorless Control of Surface-Mount Permanent-Magnet Synchronous Motors Based on a Nonlinear Observer," IEEE Trans. Ind. Electron.,* vol. 25, no. 2, pp. 290–297, Feb. 2010.